Designed Synthesis of ZnO Nanowires in Hydrothermal Process and Their Photoelectronic Nanodevice Application Towards Biomolecule Analysis

LIU Quanli

Designed Synthesis of ZnO Nanowires in Hydrothermal Process and Their Photoelectronic Nanodevice Application Towards Biomolecule Analysis

LIU Quanli

ABSTRACT

Improvement in genomic and molecular methods make it possible to identify both genetic and epigenetic mutation through microinvasive or noninvasive achieved liquid biopsies (such as blood, urine et. al.). A high-throughput, high-sensitivity and individualized detection of biomarkers in the liquid biopsy is urgently required. Technological advances in nanomaterial and nanofabrication promote the miniaturization and integration of detection units enabling realization of the requirement. This thesis has been devoted to study on designed synthesis of ZnO nanostructures towards photoelectronic nanodevice application for biomolecule analysis in liquid. Self-assembled zinc oxide nanowires are rapidly expanding their research fields in both fundamental sciences for exploring the intrinsic nanoscale properties in electrical, optical and mechanical areas, and interactive nanodevice applications e.g. molecular sensor, energy harvesting devices, biomedical/analytical devices and photoelectrical devices due to the high thermal/chemical robustness in various conditions (e.g. air, water, high temperature). Since the electrical, optical and mechanical properties of ZnO nanowires are strongly depending on the structures like morphology, crystallinity and surface characteristics, designed synthesis of nanowires are in high demand to further develop the research of ZnO nanowires. In addition, exploring the electron transport property of single ZnO nanowires enables novel design of minimized electrical nanodevice, which plays a crucial role for the development of next generation device in the up-coming IoT society.

Firstly, we demonstrate a seed layer engineering strategy to control the morphology and intrinsic crystallinity of ZnO nanowires via a hydrothermal method. The process in which nanowires grow from prepared seed template layer, additional ammonia not only promotes

growth of nanowires but also has an interaction with prepared ZnO seed template layer in initial period. Although the latter is very likely to dominate diameter, areal density and even physical property of final nanowires product, a thorough study on the function ammonia plays during initial synthesis process is lacking. We concern ammonia engineers prepared seed template layer to tailor final ZnO nanowires in areal density, diameter, length, and physical properties. Experimental results and thermodynamics simulation demonstrate two growth models of nanowires based on etch extent of prepared seed template layer. Partly etch of prepared seed layer in moderate ammonia concentration creates more nucleation sites with smaller diameter than no additional ammonia process. A rebuilding of seed templates follows completely etching of prepared one in high additional ammonia concentration status, leads to a decrease of areal density and increase of diameter. Ammonia implements transformations on seed templates realize tailoring of ZnO nanowires areal density, diameter, and even physical property.

Secondly, we explore the electron transport property of single ZnO nanowires enables novel design of minimized electrical nanodevice based on single nanowire electrical device. Ammonia-engineered seed templates and polyethyleneimine as cation surfactant to control density of the seeds were used to synthesize sparse nanowire arrays with ~120 aspect ratio at a 1 μm/h growth rate. Photolithography techniques were then used to fabricate the single nanowire device. From the ohmic contact between the ZnO nanowire and metal electrodes, nanowire resistivities were estimated to be in a range from 2.8 to 26.9 Ω·cm. Devices exhibit a ~100 (I_{UVon} / I_{UVoff}) sensitivity on exposure to ultraviolet irradiation.

Finally, atomic layer deposition (ALD) technology boosted constructure of ZnO/ Al_2O_3, ZnO/ SnO_2, and ZnO/ NiO core-shell nanowires. Nanodevices embedding the core-shell

nanowires were responded to miRNA 21 in aqueous environment. Metal oxide composites are structured to passivate ZnO nanowire surface. Thermal treatment improved nanowires crystallinity, and also optimized the nano-heterostructure. These two effects further increased the stability of nanowire, and enhanced sensing response of the sensors. Comparison of different response signal, a hypothesis was presented to further understand the sensing mechanism between metal oxide surface and miRNA. Based on a mature research of core-shell nanodevices, the selective fingerprinting of miRNAs by material-dependent nanosensors arrays is expected to realize.

CONTENTS

ABSTRACT 1

CONTENTS 4

CHAPTER I 6

General Introduction 6

1.1 General Introduction 7

1.1.1 Introduction to metal oxide nanowires 7

1.1.2 Actuality of ZnO nanowire-based devices 8

1.2 Framework for Thesis 9

1.3 References 11

CHAPTER II 17

Ammonia-Induced Seed Layer Transformations in A Hydrothermal Growth Process of Zinc Oxide Nanowires 17

2.1 Introduction 19

2.2 Experimental and thermodynamics simulation 20

2.2.1 Synthesis of ZnO nanowires 20

2.2.2 Characterization of ZnO nanostructures 21

2.2.3 Thermodynamic calculation of Zn(II) solubility in aqueous solutions 22

2.3 Result and Discussion 23

2.4 Conclusion 27

2.5 References 28

CHAPTER III 42

Photolithographically Constructed Single ZnO Nanowire Device and Its Ultraviolet Photoresponse 42

3.1 Introduction 44

3.2 Experimental 45

3.2.1 Growth and characterization of nanowires 45

3.2.2 Device fabrication 46

3.2.3 Measurement of electrical resistivity 46

3.3 Result and Discussion 47
3.4 Conclusion 50
3.5 References 50
CHAPTER IV 57
Thermal Annealing Derived Stabilization of Metal Oxide Core-shell Nanowire Towards Sensing Response to miRNA 21 57
4.1 Introduction 59
4.2 Experimental 61
4.2.1 Growth of ZnO nanowires 61
4.2.2 Core-shell nanostructures fabrication 62
4.2.3 Individual core-shell nanowire device fabrication 63
4.3 Result and Discussion 64
4.4 Conclusion 67
4.5 References 68
CHAPTER V 78
5.1 Concluding Remarks 79
5.2 Future Perspective 80
ACKNOWLEDGEMENT 82
List of publications 84

CHAPTER I

General Introduction

1.1 General Introduction

1.1.1 Introduction to metal oxide nanowires

Recently, metal-oxides are promising candidates for versatile device due to their flexible synthesis methods [1–4], high compatibility with other materials [5–8], a tremendous amount of variety [3, 9], and low-cost [10, 11]. With the development of materials synthesis and processing technologies, varied morphology and configurations of metal-oxides have been tailored, for example, thin films [9, 12], individual particles [13, 14], single crystals [12, 14], and one-dimensional nanostructures (1-D nanostructure) [15]. Among the morphology and configurations mention above, the 1-D nanostructures, especially nanowires are suited to devices integration considering of the reasons as list following: a) Their large surface-to-volume ratio makes them possess an appreciable quantity of surface atoms which are involved in surface reactions [16, 17]. b) Their surface situations would be able to regulate their electronic properties, resulting in flexible means to promote device sensitivity and selectivity [16, 17]. c) Comparing with multigranular metal oxides, the nanowires show a higher stability because of their better stoichiometry and higher crystallinity [18, 19]. d) The microscale axial direction of metal oxide nanowires conduces to potential integration with variable devices and device constructure approaches [20, 21]. e) Variety of metal oxides provides more candidates to match the sensing target and environment [3, 9]. Possessing of these significant properties, metal oxide nanowires are embedded in diverse devices represented by individual nanowire transistor, inherit the properties such as photoresponse [22], piezoelectricity [23], and chemical detection [24] while miniaturization and integration individual nanowire devices are expanded to profile physiological activity own to the high anisotropic geometry, size confinement, and

biocompatibility of metal oxide nanowires. It is predictable that combination between high density circuit integration of metal oxide nanowire devices for data acquisition and machine learning for data analysis in the fields of physical sensing, chemical detection, and medical diagnosis, would play a significant role in the process of build Internet of Things (IoT) society.

1.1.2 Actuality of ZnO nanowire-based devices

As mentioned above, semiconducting metal oxide nanowires attract substantial attention because of their extraordinary properties. Equally unsurprisingly, categories of semiconductor metal oxide nanowires have been taken into research, including nanowires composite of metal elements belong to groups II-VI, III-V, and IV [25]. Among of these, zinc oxide (ZnO) nanowires have drawn a great deal of interest due to their outstanding physical properties, various approaches of achieving, feasibility of further modified or heterojunctions with other materials, controllable morphologies, and biocompatibility [26, 27]. The well-defined lattice of single crystal ZnO nanowire shows a satisfactory response speed, sensitivity to changes of its electric surface charge, and stability in ambient conditions [27]. The listed feathers above make ZnO nanowire a potential candidate as core component embedded in diverse variety nanodevices. So far, ZnO nanowires have been used in or as light emitters, light detection applications, photovoltaic cells, photocatalytic applications, field emission, field effect transistors, chemical and biological sensors, and power nanogenerators [28]. However, the realization of industrialized applications of ZnO nanowire-based devices is still hindered by several reasons. First of all, the gap between the require of simply cost effectiveness on synthesis of large aspect ratio ZnO nanowire and the presented solutions, leaving most of the architectures remain stuck at

nanowires/nanorods array-based, which sets a limitation of taking full advantage of ZnO nanowire in the 1-D nanostructure [29]. Secondly, a fair amount of researchers flinch at the complexities in constructure of individual nanowire device. Furthermore, it is difficult for a mere ZnO nanowire to keep stability in various complicated environments, particularly in aqueous surrounding [30–33]. It is concluded that serious obstacles need to be overcome to realize wide applications of ZnO nanowires. Herein, considering of current situation of ZnO nanowires research, we establish the main objectives of the thesis, and briefly summarize as follow:

A. To develop a manageable achievement of ultralong ZnO nanowires based on unfolding ammonia function in process.
B. To build up an accessible procedure on integrating individual ZnO nanowire into devices.
C. To explore the ZnO-based individual nanowire device application towards biomolecules analysis in aqueous environment.

1.2 Framework for Thesis

This thesis is divides into five chapters, figure 1 shows the main research activities in this thesis. The first chapter begins with a general introduction about metal oxides nanowire, an extension part about current situation of ZnO-based devices, and then the framework of this thesis. From chapter II to chapter IV, we exhibit the main section of my thesis. Chapter II presents a seed layer engineering strategy to control the morphology and intrinsic crystallinity of ZnO nanowires via a hydrothermal method. The process in which nanowires grow from prepared seed template layer, ammonia is added in growth system to promotes

growth of nanowires. Although the effect of ammonia on the nanowire growth has been intensively investigated, an influence for the seed layer, which governs the initial nanowire growth, is rarely discussed. Here current part of this thesis demonstrates that ammonia strongly affects the seed layer as well as the following nanowire growth. When increasing the ammonia concentration, the nanowire density first increases and then decreases while the nanowire growth rate keeps increasing. Experimental results and thermodynamic calculations as to the initial growth process reveal that the transformation of seed layer induced by ammonia prior to the nucleation critically determines the nanowire density and thus also influences the following nanowire growth. Present results highlight the critical importance to discuss the variation of seed layer in ammonia-contained hydrothermal synthesis and suggest a novel seed engineering approach for tailoring the ZnO nanowire growth, and even physical property. In chapter III, we describe a manageable procedure to embed individual ZnO nanowire in device, and explore the electron transport property of it. Based on the results in Chapter II, sparse ZnO nanowire array with aspect ratio of ca. 120 and growth rate of 1 μm/h is synthesized by controlling density of seeds by ammonia and polyethyleneimine at initial stage of nanowire growth, and prolong the growth period by refreshing nutrient solution. The spatially-separated nanowires were cut off from growth substrate unbrokenly, and thus facilitate to construct a single-nanowire device by photolithography. The device exhibited a linear current-voltage characteristic associated with ohmic contact between ZnO nanowire and electrodes. The device further demonstrated reliable photoresponse with an I_{UV}/I_{dark} of ~100 to ultraviolet light irradiation. In chapter IV, we propose the establishment of ZnO-based individual nanodevices with high stability and sensitivity towards biomolecules analysis. The implementation approach is that, atomic

layer deposition (ALD) technology boosted constructure of ZnO/ Al_2O_3, ZnO/ SnO_2, and ZnO/ NiO core-shell nanowires. Nanodevices embedding the core-shell nanowires were responded to miRNA 21 in aqueous environment. Thermal annealing was implemented to improve nanowires stability in aqueous environment. Formation of core-shell nanostructures, on the one hand, enhanced the electrical response of ZnO nanowire to biomolecular potentially. On the other hand, thermal annealing caused diffusion of deposited metal oxide layer on ZnO nanowire surface increased stability of nanowire. Comparison of response among nanodevices with different typed of deposited metal oxide layer assisted to reveal the response mechanism. A mature research achievement on core-shell nanodevices is expected to realize selective fingerprinting of miRNAs by material-dependent nanosensors arrays. Finally, we summary the results and highlights of this thesis, and put forward the future perspectives.

1.3 References

[1] Limo, M. J.; Sola-Rabada, A.; Boix, E.; Thota, V.; Westcott, Z. C.; Puddu, V.; Perry, C. C. Interactions between Metal Oxides and Biomolecules: From Fundamental Understanding to Applications. *Chem. Rev*. **2018**, *118 (22)*, 11118–11193.

[2] Mirzaei, A.; Neri, G. Microwave-Assisted Synthesis of Metal Oxide Nanostructures for Gas Sensing Application: A Review. Sens. *Actuators B Chem*. **2016**, *237*, 749–775.

[3] Devan, R. S.; Patil, R. A.; Lin, J.-H.; Ma, Y.-R. One-Dimensional Metal-Oxide Nanostructures: Recent Developments in Synthesis, Characterization, and Applications. *Adv. Funct. Mater.* **2012**, *22 (16)*, 3326–3370.

[4] Zu, D.; Wang, H.; Lin, S.; Ou, G.; Wei, H.; Sun, S.; Wu, H. Oxygen-Deficient Metal

Oxides: Synthesis Routes and Applications in Energy and Environment. *Nano Res*. **2019**, *12 (9)*, 2150–2163.

[5] Merzlikin, S. V.; Tolkachev, N. N.; Briand, L. E.; Strunskus, T.; Wöll, C.; Wachs, I. E.; Grünert, W. Anomalous Surface Compositions of Stoichiometric Mixed Oxide Compounds. *Angew. Chem. Int. Ed*. **2010**, *49 (43)*, 8037–8041.

[6] Zhu, J.; Yin, Z.; Li, H.; Tan, H.; Chow, C. L.; Zhang, H.; Hng, H. H.; Ma, J.; Yan, Q. Bottom-Up Preparation of Porous Metal-Oxide Ultrathin Sheets with Adjustable Composition/Phases and Their Applications. *Small* **2011**, *7 (24)*, 3458–3464.

[7] Chen, J.; Huang, C.; Wu, W. Solid-State Diffusional Behaviors of Functional Metal Oxides at Atomic Scale. *Small* **2018**, *14 (6)*, 1702877.

[8] Cho, W.; Lee, Y. H.; Lee, H. J.; Oh, M. Multi Ball-In-Ball Hybrid Metal Oxides. Adv. Mater. **2011**, *23 (15)*, 1720–1723.

[9] Fortunato, E.; Barquinha, P.; Martins, R. Oxide Semiconductor Thin-Film Transistors: A Review of Recent Advances. *Adv. Mater.* **2012**, *24 (22)*, 2945–2986.

[10] Zhang, B.; Gao, P.-X. Metal Oxide Nanoarrays for Chemical Sensing: A Review of Fabrication Methods, Sensing Modes, and Their Inter-Correlations. *Front. Mater*. **2019**, *6*, 55.

[11] Mao, Y.; Park, T.-J.; Zhang, F.; Zhou, H.; Wong, S. S. Environmentally Friendly Methodologies of Nanostructure Synthesis. *Small* **2007**, *3 (7)*, 1122–1139.

[12] Nomura, K. Thin-Film Transistor Fabricated in Single-Crystalline Transparent Oxide Semiconductor. *Science* **2003**, *300 (5623)*, 1269–1272.

[13] Zhang, H.; Ji, Z.; Xia, T.; Meng, H.; Low-Kam, C.; Liu, R.; Pokhrel, S.; Lin, S.; Wang, X.; Liao, Y.-P.; Wang, M.; Li, L.; Rallo, R.; Damoiseaux, R.; Telesca, D.; Mädler, L.;

Cohen, Y.; Zink, J. I.; Nel, A. E. Use of Metal Oxide Nanoparticle Band Gap To Develop a Predictive Paradigm for Oxidative Stress and Acute Pulmonary Inflammation. *ACS Nano* **2012**, *6 (5)*, 4349–4368.

[14] Li, Z.; Li, H.; Wu, Z.; Wang, M.; Luo, J.; Torun, H.; Hu, P.; Yang, C.; Grundmann, M.; Liu, X.; Fu, Y. Advances in Designs and Mechanisms of Semiconducting Metal Oxide Nanostructures for High-Precision Gas Sensors Operated at Room Temperature. *Mater. Horiz.* **2019**, *6 (3)*, 470–506.

[15] Arafat, M. M.; Dinan, B.; Akbar, S. A.; Haseeb, A. S. M. A. Gas Sensors Based on One Dimensional Nanostructured Metal-Oxides: A Review. *Sensors* **2012**, *12 (6)*, 7207–7258.

[16] Lien, D.-H.; Durán Retamal, J. R.; Ke, J.-J.; Kang, C.-F.; He, J.-H. Surface Effects in Metal Oxide-Based Nanodevices. *Nanoscale* **2015**, *7 (47)*, 19874–19884.

[17] Chen, X.; Wong, C. K. Y.; Yuan, C. A.; Zhang, G. Nanowire-Based Gas Sensors. *Sens. Actuators B Chem.* **2013**, *177*, 178–195.

[18] Comini, E.; Sberveglieri, G. Metal Oxide Nanowires as Chemical Sensors. *Mater. Today* **2010**, *13 (7–8)*, 36–44.

[19] Comini, E.; Baratto, C.; Faglia, G.; Ferroni, M.; Ponzoni, A.; Zappa, D.; Sberveglieri, G. Metal Oxide Nanowire Chemical and Biochemical Sensors. *J. Mater. Res.* **2013**, *28 (21)*, 2911–2931.

[20] Kolmakov, A.; Moskovits, M. Chemical Sensing and Catalysis by One-Dimensional Metal-Oxide Nanostructures. *Annu. Rev. Mater. Res.* **2004**, *34 (1)*, 151–180.

[21] Shen, G.; Chen, P.-C.; Ryu, K.; Zhou, C. Devices and Chemical Sensing Applications of Metal Oxide Nanowires. *J Mater Chem* 2009, *19 (7)*, 828–839.

[22] Ouyang, W.; Teng, F.; He, J.-H.; Fang, X. Enhancing the Photoelectric Performance of Photodetectors Based on Metal Oxide Semiconductors by Charge-Carrier Engineering. *Adv. Funct. Mater*. **2019**, *29 (9)*, 1807672.

[23] He, J. H.; Hsin, C. L.; Liu, J.; Chen, L. J.; Wang, Z. L. Piezoelectric Gated Diode of a Single ZnO Nanowire. *Adv. Mater*. **2007**, *19 (6)*, 781–784.

[24] Po-Chiang Chen; Guozhen Shen; Chongwu Zhou. Chemical Sensors and Electronic Noses Based on 1-D Metal Oxide Nanostructures. *IEEE Trans. Nanotechnol*. **2008**, *7 (6)*, 668–682.

[25] Chang, P.-C.; Lu, J. G. ZnO Nanowire Field-Effect Transistors. *IEEE Trans. Electron Devices* **2008**, *55 (11)*, 2977–2987.

[26] Janotti, A.; Van de Walle, C. G. Fundamentals of Zinc Oxide as a Semiconductor. *Rep. Prog. Phys*. **2009**, *72 (12)*, 126501.

[27] Rackauskas, S.; Barbero, N.; Barolo, C.; Viscardi, G. ZnO Nanowire Application in Chemoresistive Sensing: A Review. *Nanomaterials* **2017**, *7 (11)*, 381.

[28] Witkowski, B. Applications of ZnO Nanorods and Nanowires - A Review. *Acta Phys. Pol. A* **2018**, *134 (6)*, 1226–1246.

[29] Lupan, O.; Cretu, V.; Postica, V.; Ahmadi, M.; Cuenya, B. R.; Chow, L.; Tiginyanu, I.; Viana, B.; Pauporté, T.; Adelung, R. Silver-Doped Zinc Oxide Single Nanowire Multifunctional Nanosensor with a Significant Enhancement in Response. *Sens. Actuators B Chem*. **2016**, *223*, 893–903.

[30] Blesa, M. A.; Weisz, A. D.; Morando, P. J.; Salfity, J. A.; Magaz, G. E.; Regazzoni, A. E. The Interaction of Metal Oxide Surfaces with Complexing Agents Dissolved in Water. Coord. *Chem. Rev*. **2000**, *196 (1)*, 31–63.

[31] Meyer, B.; Marx, D.; Dulub, O.; Diebold, U.; Kunat, M.; Langenberg, D.; Wöll, C. Partial Dissociation of Water Leads to Stable Superstructures on the Surface of Zinc Oxide. *Angew. Chem. Int. Ed.* **2004**, *43 (48)*, 6641–6645.

[32] Zhou, J.; Xu, N. S.; Wang, Z. L. Dissolving Behavior and Stability of ZnO Wires in Biofluids: A Study on Biodegradability and Biocompatibility of ZnO Nanostructures. *Adv. Mater.* **2006**, *18 (18)*, 2432–2435.

[33] Dumontel, B.; Canta, M.; Engelke, H.; Chiodoni, A.; Racca, L.; Ancona, A.; Limongi, T.; Canavese, G.; Cauda, V. Enhanced Biostability and Cellular Uptake of Zinc Oxide Nanocrystals Shielded with a Phospholipid Bilayer. *J. Mater. Chem. B* **2017**, *5 (44)*, 8799–8813.

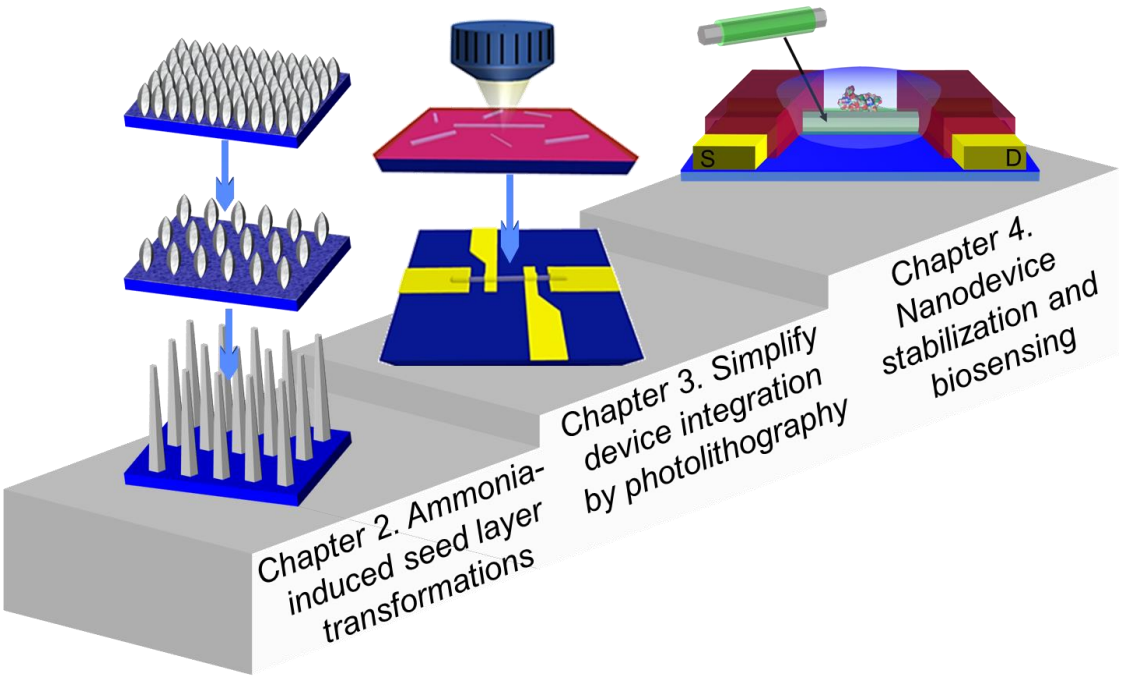

Figure 1 Framework for this thesis.

CHAPTER II

Ammonia-Induced Seed Layer Transformations in A Hydrothermal Growth Process of Zinc Oxide Nanowires

Chapter II presents a seed layer engineering strategy to control the morphology and intrinsic crystallinity of ZnO nanowires via a hydrothermal method. Although the effect of ammonia on the nanowire growth has been intensively investigated, an influence for the seed layer, which governs the initial nanowire growth, is rarely discussed. Here, Chapter II demonstrates that ammonia strongly affects the seed layer as well as the following nanowire growth. When increasing the ammonia concentration, the nanowire density first increases and then decreases while the nanowire growth rate keeps increasing. Experimental results and thermodynamic calculations as to the initial growth process reveal that the transformation of seed layer induced by ammonia prior to the nucleation critically determines the nanowire density and thus also influences the following nanowire growth. Present results highlight the critical importance to discuss the variation of seed layer in ammonia-contained hydrothermal synthesis and suggest a novel seed engineering approach for tailoring the ZnO nanowire growth.

Ammonia-Induced Seed Layer Transformations in A Hydrothermal Growth Process of Zinc Oxide Nanowires

2.1 Introduction

Single crystalline zinc oxide (ZnO) nanowires have recently been extending their application fields from previous optics and electronics to newly emerging nano-bio analysis due to the various fascinating features including wide direct bandgap [1, 2], large exciton binding energy [1-3], piezoelectricity [4,5], Lewis acidity [6, 7], high isoelectric point [8] and biocompatibility [9, 10]. Thanks to such variety of features, unique devices including light emitting diode (LED), nanogenerator, bio/chemical sensors and biomedical analysis devices have been demonstrated so far using ZnO nanowires [11-15]. A hydrothermal synthesis is among the most broadly utilized technique for fabricating the ZnO nanowires [16-18]. This is because the hydrothermal process is conducted at low temperature less than 100 ºC and the diameter/position of nanowires are designable via seed crystals. These allow us to integrate the ZnO nanowires with various materials and devices on a substrate [19, 20]. Fundamentally, the anisotropic crystal growth of ZnO nanowires originates from a preferential nucleation on ZnO (0001) plane, which is dominated by zinc hydroxide complexes ($Zn(OH)_n$) precursor [21-23]. Ammonia is a well-known additive to promote the ZnO nanowire growth [24-28]. Such ammonia effect has been interpreted in terms of the variations of ionic species in aqueous solution and their electrostatic interactions with ZnO crystal planes [22, 29]. Recent study by Sakai *et al.* further revealed that the increase of growth rate is mainly due to the change of rate limiting

process from the precursor diffusion process to the ligand exchange process, which is caused by the decreased concentration of $Zn(OH)_n$ [21]. On the other hand, the ammonia causes a dissociation of ZnO during the nanowire growth. The sharp and uniformly-shaped nanowire tips were formed as a result of ammonia-induced face-selective etching on ZnO $\{10\bar{1}1\}$ planes [30,31]. By using this etching effect, Zhao *et al.* demonstrated the synthesis of monodispersedly sized ZnO nanowires from randomly sized seeds [31]. The role of ammonia on the nanowire growth has been intensively investigated as described above, however, an influence for the seeds, which govern the nanowire growth, is rarely discussed. Clarifying how ammonia influences the seeds is of crucial importance to comprehensively understand and tailor the ammonia-induced ZnO nanowire growth. Thus, in our experiment design, different quantity of ammonia (200 mM, 400 mM, 600 mM, 800 mM, 1000 mM) are added into nutrient solution within fixed $Zn(NO_3)_2$ and methenamine (HMTA) concentration, respectively. Without control of any other parameter such as pH and temperature, we mainly focus our attention on ammonia interventional reconstruct of seed templates during initial 30 min of hydrothermal process. In this study, we investigate the ammonia effect on seeds in hydrothermal synthesis of ZnO nanowires. We found that ammonia transforms the seed layer prior to nucleation and strongly affects the following nanowire growth.

.

2.2 Experimental and thermodynamics simulation

2.2.1 Synthesis of ZnO nanowires

ZnO nanowire growth was conducted by a hydrothermal synthesis. First, 20 mm × 10 mm silicon substrates (N-type) were cleaned in a mixture of 98 % sulfuric acid and 35 %

hydrogen peroxide with volume ratio of 3:1 at 180 ºC for 2 h. After cooling down to room temperature, the substrates were taken out from the cleaning solution, washed by ultrapure water and dried by blowing nitrogen gas. The ZnO seed layer was then deposited on the substrate by radio frequency (RF) sputtering with RF power of 50 W under ambient pressure of 1 Pa with $Ar:O_2$ ratio of 5:1 at room temperature. The deposition rate of ZnO seed layer was 10 nm/ min. The thickness of ZnO seed layer was controlled to be 75 nm, where the highest areal density of uniformly shaped nanowires is available (see Figure 2-1). The nanowire growth solution was prepared by mixing zinc nitrate hexahydrate ($Zn(NO_3)_2 \cdot 6H_2O$, 40 mM), hexamethylenetetramine (HMTA, 40 mM) and ammonia solution (25 wt.%) with varying the concentration in a range of 0-1000 mM at room temperature. The seed layer coated substrates were immersed into Teflon cups filled with 50 ml of growth solution in a manner of upside down. Then the Teflon cups were put into the oven set at 95 ºC. The growth time was varied in between 10-180 min. After the growth, the samples were washed by ultrapure water and acetone, then dried at 80 °C for 10 min.

2.2.2 Characterization of ZnO nanostructures

The morphologies of ZnO seed layer and ZnO nanowires were evaluated by a scanning electron microscope (SEM; Zeiss Supra 40 VP). The ZnO nanostructures constructed at early stage were characterized by a grazing-incidence x-ray diffraction (GI-XRD; Rigaku FR-E). For GI-XRD, a radiation source of Cu Kα ($\lambda = 0.154$ nm) was used and the incident angle of the beam to the sample surface was adjusted at about 0.18−0.22º.

2.2.3 Thermodynamic calculation of Zn(II) solubility in aqueous solutions

The solubility of Zn(II) (y axes) calculate from relevant chemical equilibria is the maximum concentration of zinc ions without precipitating ZnO in solution, that is, the total concentration of zinc ions in all soluble zinc-containing compounds at equilibrium.

Consider the relevant reaction

$$\boldsymbol{aA + bB \rightleftharpoons cC + dD},$$

(1.1)

for which

$$\boldsymbol{K_{eq} = \frac{[C]^c[D]^d}{[A]^a[B]^b}}.$$

(1.2)

This relationship is known as the law of mass action, where K_{eq} is the equilibrium constant for the reaction 1.1. In 1.2, [A], [B], [C] and [D] are activities of each species (in dilute solution, the activity is assumed to be equal to equilibrium concentration approximatively); a, b, c and d are stoichiometric numbers. Known the equilibrium constant K_{eq} at 298.15 K (25 ºC) refer to [29] and [32], all the concentrations of zinc-containing compounds as a function of temperature, pH, and total ammonia concentration can be solved. The solubility of ZnO is then calculated as the sum of the concentration of zinc ions in all soluble zinc-containing compounds at equilibrium.

For the solubility of ZnO at other temperatures (e.g., 333.15 K in this work), we calculate the K_{eq} from

$$\boldsymbol{ln\frac{K_{eq(T_2)}}{K_{eq(T_1)}} = -\frac{\Delta_r H_m^{\Theta}}{R}\left(\frac{1}{T_2} - \frac{1}{T_1}\right)},$$

(1.3)

where $K_{eq(T_1)}$ is defined as equilibrium constant at temperature T_1, $K_{eq(T_2)}$ is defined as equilibrium constant at temperature T_2; $\Delta_r H_m^{\Theta}$ is standard molar reaction enthalpy change. According to Hess's Law

$$\boldsymbol{\Delta_r H_m^{\Theta} = \sum_B \left[\mu_B \Delta_f H_m^{\Theta}(B)\right]},$$

(1.4)

where $\Delta_f H_m^{\Theta}$ is enthalpy of formation, μ_B is stoichiometric number. We assume that $\Delta_r H_m^{\Theta}$ is independent of temperature, which is often a very reasonable approximation. In current work, we obtain the K_{eq} at 333.15 K (60 ºC) base on known K_{eq} at 298.15 K (25 ºC.) and calculated $\Delta_r H_m^{\Theta}$, and then calculate the sum of zinc ions concentration at 333.15 K.

2.3 Result and Discussion

Figure 2-2A shows the cross-sectional SEM images of ZnO nanowires grown for 3 h with varying ammonia concentration (C_{NH3}) of 0-1000 mM. When increasing C_{NH3}, the nanowire growth rate increases. The observed trend is consistent with many previous studies, which can be interpreted in terms of the variations of ionic species in aqueous solution, their electrostatic interactions with ZnO crystal planes and the rapid ligand exchange process between different zinc complexes [21-28]. On the other hand, the areal number density of nanowire (hereafter nanowire density) and the diameter show unique trends as explained in the followings. Figure 2-2B shows the quantitative C_{NH3}

dependences on the nanowire density and the diameter. We found that the nanowire density tends to first increase and then decrease with increasing C_{NH3}, and the diameter inversely correlates with the nanowire density. These trends cannot be explained by the ammonia-induced crystal growth promotion. Although the diameter is affected by various factors, the observed correlation indicates that the diameter is predominantly determined by a material competition effect between adjacent nanowires [32]. Thus, these results show that ammonia affects not only the nanowire growth rate but also the nanowire density and the diameter.

We found that the seed layer located at the bottom of nanowires tends to be thinner with increasing C_{NH3}, as shown in figure 2-2A and 2-2C. This result indicates the significant effect of ammonia on the seed layer and therefore strongly recommends to observe the seed layer at the initial growth process, although it has been rarely discussed previously. Figure 2-3A shows SEM images of the seed layer observed after 10-30 min of growth process with various C_{NH3}. At relatively low C_{NH3} range of 0-600 mM, the nanowire growth immediately occurs within 20 min. In this condition, the nanowire density tends to increase with increasing C_{NH3}. On the other hand, at relatively high C_{NH3} range of 800-1000 mM, the seed layer seems to be removed from the substrate and none of nanowire growth can be seen. We found that the seed layer is removed within first 10 min and the nanoparticles tend to form in the following 20 min. The variations of nanowire/nanoparticle density observed at the initial growth process is consistent with that of the nanowire density in figure 2-2B, suggesting that the nanowire density is determined by the morphology of seed layer formed at the initial growth process. Thus, the result in figure 2-3A clearly evidences that ammonia strongly affects the seed layer at initial growth process as well as the

following nanowire growth.

Here we consider how ammonia affects the seed layer at the initial growth process. First, we discuss the increasing trend of nanowire density with increasing C_{NH3} at relatively low concentration range. Since the seed layer fully covers the substrate in this C_{NH3} range, the variation of nanowire density should be determined by the nucleation phenomena on the seed layer. As seen in figure 2-3A, a nanowire is grown from several seed crystals at C_{NH3} 0 mM while it tends to grow from individual seed crystal by increasing C_{NH3}. This trend can be interpreted in terms of the suppression of nuclei merge via ammonia induced sharp tip formation as demonstrated by our previous study.[31] When using the densely deposited seed crystals, the adjacent nuclei spontaneously merge during the nanowire growth and this leads to the decrease of nanowire density. In the previous study, we found that the sharp tip seeds formed by ammonia-based etching provide the spatially separated nucleation sites and suppress the merge of nuclei. Since the sharp tip formation on seeds is promoted by increasing C_{NH3}, this might lead the increase of nanowire density at relatively low concentration range.

Next, we discuss the decreasing trend of nanowire density with increasing C_{NH3} at relatively high concentration range. According to the results in figure 2-2C and 2-3A, we assume that the seed layer is dissociated prior to the nucleation and the number of remaining seeds might determine the nanowire density. In fact, the pH becomes over 11 by introducing 800 mM ammonia (see figure 2-4), which is high enough for dissociating ZnO [31, 33]. Figure 2-3B shows the Zn mapping of seed layers characterized by energy dispersive spectroscopy (EDS). The images were taken from the initial seed layer and after 10-30 min of growth process with various C_{NH3} (the all data is shown in figure 2-5). We

found that the seeds are inhomogeneously distributed at C_{NH3} 800 mM and only the sparsely distributed nanoparticles are seen at C_{NH3} 1000 mM. More specifically, the relative Zn intensity normalized by the initial ZnO seed layer decreases by 88-90 % after 10 min of growth process at C_{NH3} 800-1000 mM (figure 2-3C). These results clearly evidence that the seed layer is dissociated during initial growth process at relatively high C_{NH3} range.

We also found in figure 2-3B that the seed density increases by extending the growth time to 30 min, which is consistent with the result in figure 3A and confirmed as the variation of Zn intensity in figure 2-3C. In order to specify the variation of seed crystals observed above, we performed GI-XRD measurement with varying the growth time in figure 2-3D. In this experiment, the samples of C_{NH3} 800 mM were evaluated. There found two trends as to the variation of seed crystals. First, when increasing the growth time, the ZnO (002) peak intensity initially decreases at 10 min and then increases at 30 min as consistent with results in figure 2-3A-C. This indicates that the seed crystals are reconstructed after the dissociation. Second, although only the ZnO (002) peak is observable in the initial seed layer, (100) peak and (101) peak also tend to appear with increasing the growth time, showing that the variously oriented seed crystals are reconstructed after the dissociation. Such reconstructed seed crystals led to the variety of orientation in the nanowires grown at high C_{NH3} condition (see figure 2-2A). Note that the seed density at 30 min of growth time is very similar to that observed in figure 2-2A. Thus, these results highlight that the nanowire density at high C_{NH3} condition is strongly governed via dissociation and reconstruction of seed crystals.

To gain the in-depth insight for the experimental results observed above, we performed the thermodynamic calculations at given growth conditions. In this calculation, the

solubility of ZnO, i.e. the saturated Zn concentration, was estimated by involving all of related zinc ions existing in the growth solution. The details of calculation are seen in experiment section. The pH value and the temperature of growth solution were measured at each growth time and utilized for estimating the solubility (see figure 2-4). Figure 2-6A and 2-6B respectively show the pH dependent solubility of ZnO with various C_{NH3} at 25 ºC and 60 ºC, where 60 ºC is associated with the growth time of 10-20 min. Note that the dotted lines and the filled circles in the figures represent the Zn concentration used for the nanowire growth and the solubility of ZnO at the measured pH condition, respectively. At relatively low C_{NH3} range (i.e. 400-600 mM), the growth solution is almost saturated at 25 ºC and supersaturated at 60 ºC. This result shows the good consistency with the results of figure 3A, of which the nanowire growth immediately occurs after 10 min of growth time at this condition. Contrary, at relatively high C_{NH3} range (i.e. 800-1000 mM), the growth solution is not saturated and afford to dissociate ZnO at 25 ºC while it becomes supersaturated by increasing temperature up to 60 ºC. Such temperature dependence observed at higher C_{NH3} range is consistent with previous study, where $Zn(NH_3)_4^{2+}$ ions dominate the solubility of ZnO in ammonia-added aqueous solution.[22] In fact, our calculations revealed that the solubility of ZnO in our experimental conditions is governed by the concentration of $Zn(NH_3)_4^{2+}$ ions (see figure 2-7). Thus the dynamic change of saturation degree induced by temperature variation reasonably explain why the seed layer is dissociated at first and then reconstructed during the initial growth process.

2.4 Conclusion

In conclusion, we investigated the effect of ammonia on the seed layer in hydrothermal synthesis of ZnO nanowires, which had been rarely discussed previously. The nanowire

growth rate increased accompanying with the increase of C_{NH3} as consistent with many previous studies. On the contrary, the nanowire density and the diameter exhibited the unique tendencies, of which the nanowire density first increased then decreased with increasing C_{NH3} and the diameter inversely correlated with the nanowire density. The detailed experimental analysis revealed that the transformation of seed layer occurs prior to the nucleation and critically determines the features of fabricated nanowires including the nanowire density and the diameter. There found that the nanowire density is governed by two dominant transformations of the seed layer, i.e. the formation of sharp tips on the seed increases the nanowire density by suppressing the merge of adjacent nuclei at relatively low C_{NH3} range, and the dissociation of seed layer decreases the nanowire density at relatively high C_{NH3} range. We also found that at relatively high C_{NH3} range the seed crystals were reconstructed after the dissociation. Thermodynamic calculation revealed that the variation of saturation degree at initial growth process is responsible for the reconstruction of seed crystals. Our results highlight that observing the variation of seed layer at initial growth process is of critical importance to understand the comprehensive growth mechanism in ammonia-contained hydrothermal ZnO nanowire synthesis, and also suggest a novel seed engineering approach for tailoring the ZnO nanowire growth.

2.5 References

[1] Xu, S.; Wang, Z. L. One-dimensional ZnO nanostructures: Solution growth and functional properties. *Nano Res.* **2011**, *4*, 1013-1098.

[2]Özgür, Ü.; Alivov, Y. I.; Liu, C.; Teke, A.; Reshchikov, M. A.; Doğan, S.; Avrutin, V.; Cho, S. J.; Morkoç, H. A comprehensive review of ZnO materials and devices. *J. Appl. Phys.* **2005**, *98*, 041301.

[3]Thomas, D. G. The exciton spectrum of zinc oxide. *J. Phys. Chem. Solids* **1960**, *15*, 86-96.

[4]Wang, Z. L.; Song, H. Piezoelectric nanogenerators based on zinc oxide nanowire arrays. *Science* **2006**, *312*, 242-246.

[5]Groo, L.; Inman, D. J.; Sodano, H. A. In situ damage detection for fiber-reinforced composites using integrated zinc oxide nanowires. *Adv. Funct. Mater.* **2018**, *28*, 1802846.

[6]Ballerini, G.; Ogle, K.; Barthés-Labrousse, M.-G. The acid–base properties of the surface of native zinc oxide layers: An XPS study of adsorption of 1,2-diaminoethane. *Appl. Surf. Sci.* **2007**, *253*, 6860-6867.

[7]Perez-Lopez, Q. W.; Farias, A. C.; Marcilio, N. R.; Bueno, J. M. C. The catalytic behavior of zinc oxide prepared from various precursors and by different methods. *Mater. Res. Bull.* **2005**, *40*, 2089-2099.

[8]Cao, L.; Kiely, J.; Piano, M.; Luxton, R. Facile and inexpensive fabrication of zinc oxide based bio-surfaces for C-reactive protein detection. *Sci. Rep.* **2018**, *8*, 12687.

[9]Dagdeviren, C.; Hwang, S.-W.; Su, Y.; Kim, S.; Cheng, H.; Gur, O.; Haney, R.; Omenetto, F. G.; Huang, Y.; Rogers, J. A. Transient, Biocompatible electronics and energy harvesters based on ZnO. *Small* **2013**, *9*, 3398-3404.

[10] Bhang, S. H.; Jang, W.; Han, J.; Yoon, J.-K.; La, W.-G.; Lee, E.; Kim, Y. S.; Shin, J.-Y.; Lee,T.-J.; Baik, H. K.; Kim, B.-S. Zinc oxide nanorod-based piezoelectric dermal patch for wound healing. *Adv. Funct. Mater.* **2017**, *27*, 1603497.

[11] Bao, J.; Zimmler, M. A.; Capasso, F.; Wang, X.; Ren, Z. F. Broadband ZnO single-nanowire light-emitting diode. *Nano Lett.* **2006**, *6*, 1719-1722.

[12] Wang, X.; Song, J.; Liu, J.; Wang, Z. L. Direct-current nanogenerator driven by ultrasonic waves. *Science* **2007**, *316*, 102-105.

[13] Haarindraprasad, R.; Hashim, U.; Gopinath, S. C. B.; Perumal, V.; Liu, W.-W.; Balakrishnan, S. R. Fabrication of interdigitated high-performance zinc oxide nanowire modified electrodes for glucose sensing. *Anal. Chim. Acta* **2016**, *925*, 70-81.

[14] Xu, X.; Yan, M.; Tian, X.; Yang, C.; Shi, M.; Wei, Q.; Xu, L.; Mai, L. In situ investigation of Li and Na ion transport with single nanowire electrochemical devices. *Nano Lett.* **2015**, *15*, 3879-3884.

[15] Yasui, T.; Yanagida, T.; Ito, S.; Konakade, Y.; Takeshita, D.; Naganawa, K.; Nagashima, K.; Shimada, T.; Kaji, N.; Nakamura, Y.; Thiodorus, I. A.; He, Y.; Rahong, S.; Kanai, M.; Yukawa, H.; Ochiya, T.; Kawai, T.; Baba, Y. Unveiling massive numbers of cancer-related urinary-microRNA candidates via nanowires. *Sci. Adv.* **2017**, *3*, e1701133.

[16] Cheng, J. J.; Nicaise, S. M.; Berggren, K. K.; Gradečak, S. Dimensional tailoring of hydrothermally grown zinc oxide nanowire arrays. *Nano Lett.* **2016**, *16*, 753-759.

[17] Cho, J.; Salleh, N.; Blanco, C.; Yang, S.; Lee, C.; Kim, Y.; Kim, J.; Liu, J. Novel synthetic methodology for controlling the orientation of zinc oxide nanowires grown on silicon oxide substrates. *Nanoscale* **2014**, *6*, 3861-3867.

[18] Qiu, J.; Li, X.; He, W.; Park, S.-J.; Kim, H.-K.; Hwang, Y.-H.; Lee, J.-H.; Kim, Y.-D. The growth mechanism and optical properties of ultralong ZnO nanorod arrays with a high aspect ratio by a preheating hydrothermal method. *Nanotechnology* **2009**, *20*, 155603.

[19] Ou, C.; Sanchez-Jimenez, P.; Datta, A.; Boughey, F. L.; Whiter, R. A.; Sahonta, S. L.; Kar-Narayan, S. Template-assisted hydrothermal growth of aligned zinc oxide nanowires for piezoelectric energy harvesting applications. *ACS Appl. Mater. Inter.* **2016**, *8*, 13678-13683.

[20] Azzouz, I.; Habba, Y. G.; Capochichi-Gnambodoe, M.; Marty, F.; Vial, J.; Leprince-Wang, Y.; Bourouina, T. Zinc oxide nano-enabled microfluidic reactor for water purification and its applicability to volatile organic compounds. *Microsyst. Nanoeng.* **2018**, *4*, 17093.

[21] Sakai, D.; Nagashima, K.; Yoshida, H.; Kanai, M.; He, Y.; Zhang, G.; Zhao, X.; Takahashi, T.; Yasui, T.; Hosomi, T.; Uchida, Y.; Takeda, S.; Baba, Y.; Yanagida, T. Substantial narrowing on the Width of "concentration Window" of hydrothermal ZnO nanowires via ammonia addition. *Sci. Rep.* **2019**, *9*, 14160.

[22] He, Y.; Yanagida, T.; Nagashima, K.; Zhuge, F.; Meng, G.; Xu, B.; Klamchuen, A.; Rahong, S.; Kanai, M.; Li, X.; Suzuki, M.; Kai, S.; Kawai, T. Crystal-plane dependence of critical concentration for nucleation on hydrothermal ZnO nanowires. *J. Phys. Chem. C* **2013**, *117*, 1197-1203.

[23] Cossuet, T.; Appert, E.; Thomassin, J.-L.; Consonni, V. Polarity-dependent growth rates of selective area grown ZnO nanorods by chemical bath deposition. *Langmuir* **2017**, *33*, 6269-6279.

[24] Syrrokostas, G.; Govatsi, K.; Yannopoulos, S. N. High-quality, reproducible ZnO nanowire arrays obtained by a multiparameter optimization of chemical bath deposition growth. *Cryst. Growth Des.* **2016**, *16*, 2140-2150.

[25] Richardson, J. J.; Lange, F. F. Controlling low temperature aqueous synthesis of ZnO. 2. A novel continuous circulation reactor. *Cryst. Growth Des.* **2009**, *9*, 2576-2581.

[26] Kwon, T. H.; Kim, K.; Park, S. H.; Annamalai, A.; Lee, M. J. Effect of seed particle size and ammonia concentration on the growth of ZnO nanowire arrays and their photoconversion efficiency. *Int. J. Nanotechnol.* **2013**, *10*, 681-691.

[27] Boubenia, S.; Dahiya, A. S.; Poulin-Vittrant, G.; Morini, F.; Nadaud, K.; Alquier, D. A facile hydrothermal approach for the density tunable growth of ZnO nanowires and their electrical characterizations. *Sci. Rep.* **2017**, *7*, 15187.

[28] Chen, L.-Y.; Yin, Y.-T.; Chen, C.-H.; Chiou, J.-W. Influence of polyethyleneimine and ammonium on the growth of ZnO nanowires by hydrothermal method. *J. Phys. Chem. C* **2011**, *115*, 20913-20919.

[29] Richardson, J. J.; Lange, F. F. Controlling low temperature aqueous synthesis of ZnO. 1. Thermodynamic analysis. *Cryst. Growth Des.* **2009**, *9*, 2570-2575.

[30] Wang, H. Q.; Li, G. H.; Jia, L. C.; Wang, G. Z.; Li, L. General in situ chemical etching synthesis of ZnO nanotips array. *Appl. Phys. Lett.* **2008**, *93*, 153110.

[31] Zhao, X.; Nagashima, K.; Zhang, G.; Hosomi, T.; Yoshida, H.; Akihiro, Y.; Kanai, M.; Mizukami, W.; Zhu, Z.; Takahashi, T.; Suzuki, M.; Samransuksamer, B.; Meng, G.; Yasui, T.; Aoki, Y.; Baba, Y.; Yanagida, T. Synthesis of monodispersedly sized ZnO nanowires from randomly sized seeds. *Nano Lett.* **2020**, *20*, 599-605.

[32] Lee, J. M.; No, Y.-S.; Kim, S.; Park, H.-G.; Park, W. I. Strong interactive growth behaviours in solution-phase synthesis of three-dimensional metal oxide nanostructures. *Nat. Commun.* **2015**, *6*, 6325.

[33] Zhou, J. Xu, N. S.; Wang, Z. L. Dissolving behavior and stability of ZnO wires in biofluids: A study on biodegradability and biocompatibility of ZnO nanostructures. *Adv. Mater.* **2006**, *18*, 2432-2435.

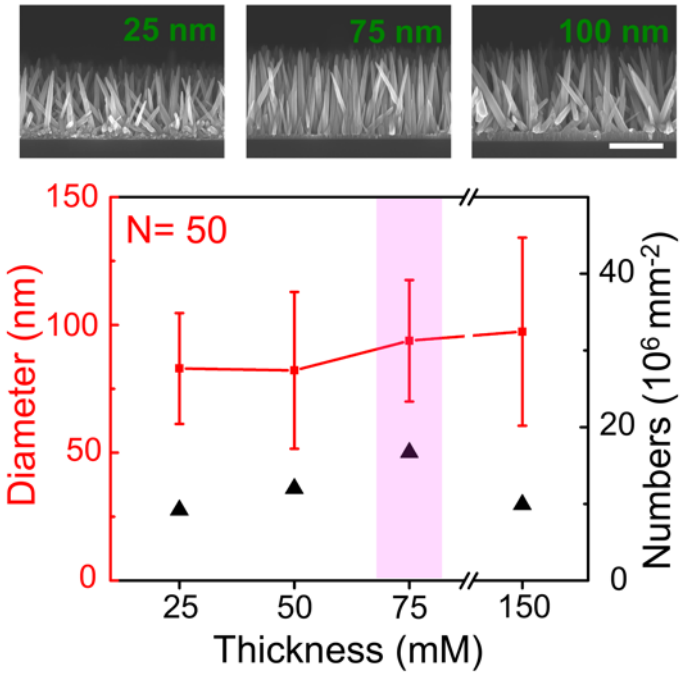

Figure 2-1 SEM images, diameter and areal density of ZnO nanowires grown with various seed layer thickness. The data was taken with growth time for 3 h and without NH_3. (scale bar = 1 μm).

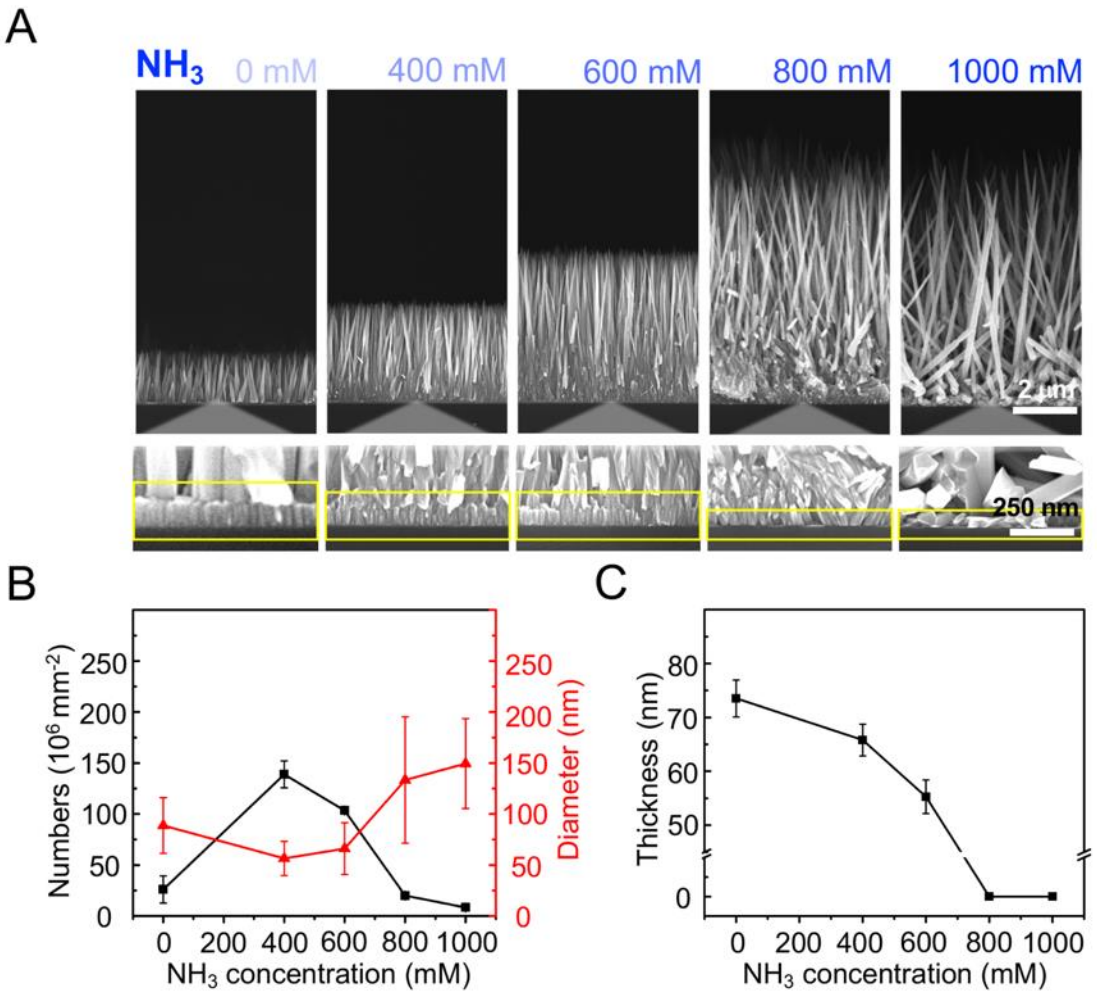

Figure 2-2. SEM images and statistical analysis of nanowires grown in various concentrations of ammonia after growth time for 3 h. **A.** Nanostructure morphology variation from horizontal direction with increase of ammonia concentrations. Yellow squares are enlarged views of nanowire roots. Images in the same row use the same scale bars. **B**. Nanowire areal density and diameter in various concentrations of ammonia. Error bars show the standard deviation for a series of measurements (for nanowires number: N = 10, for diameter: N= 100). **C**. Thickness of ZnO seed layer in various concentrations of ammonia. Error bars show the standard deviation for a series of measurements (N = 3).

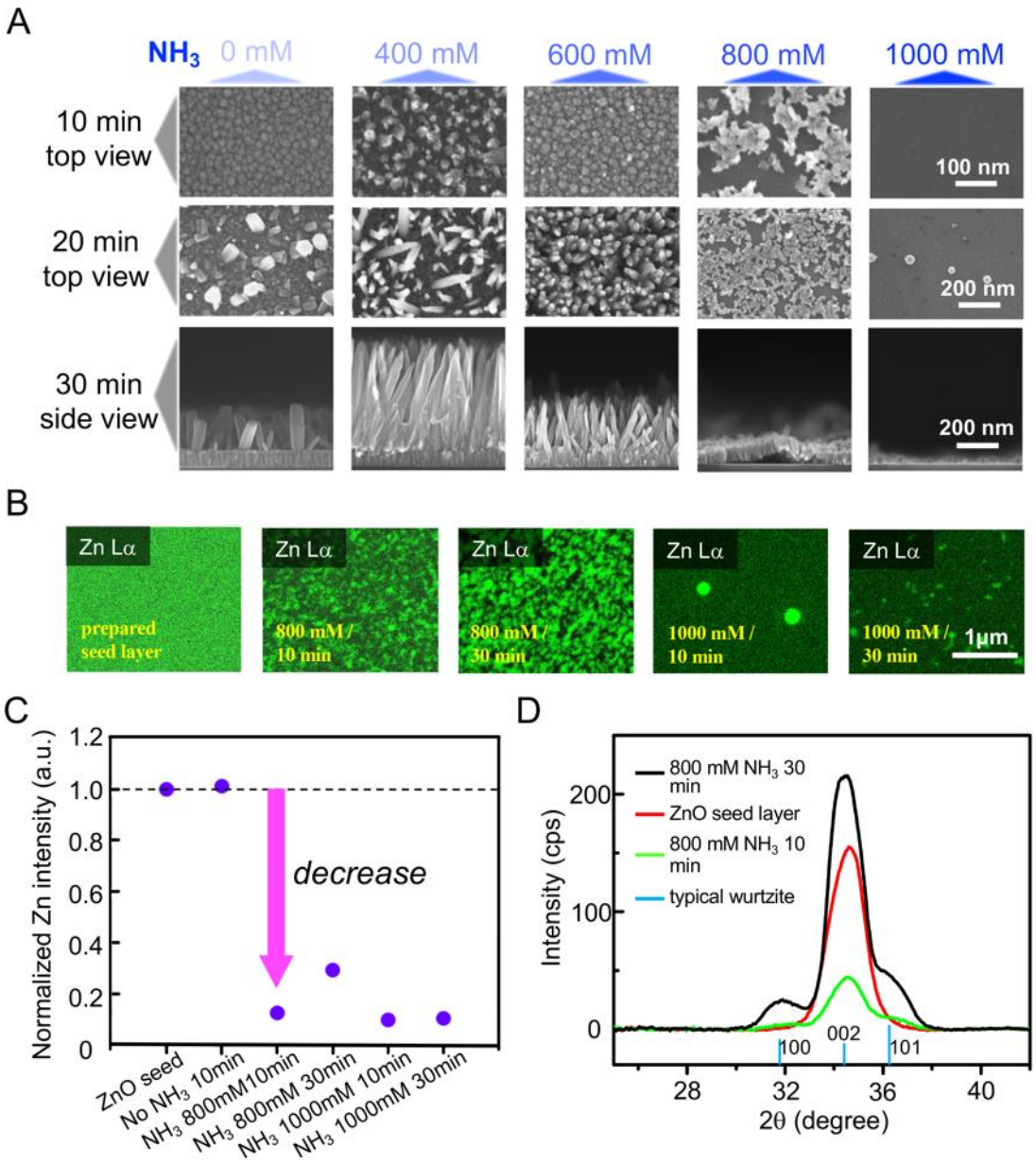

Figure 2-3. Characteristics of ZnO seed layers. **A**. SEM images of synthesis products at the initial 10, 20 and 30 min. Product morphologies varied with increase of ammonia concentrations. Images in the same row have the same scale bar as given in the last image of the row. **B**. EDS mapping analysis of seed layer transformation after immersing into growth solution with 800 and 1000 mM ammonia for 10 and 30 min respectively. **C**. Normalized Zn intensity of the substrate during the initial 30 min of the hydrothermal

process. Images have the same scale bar as given in the last image of the row. **D**. GI-XRD profiles of prepared ZnO seed layer and prepared ZnO seed layer after immersing into growth solution with 800 mM ammonia addition for 10 and 30 min. Vertical light blue lines indicate typical wurtzite (JCPDS NO. 36- 1451) peak positions.

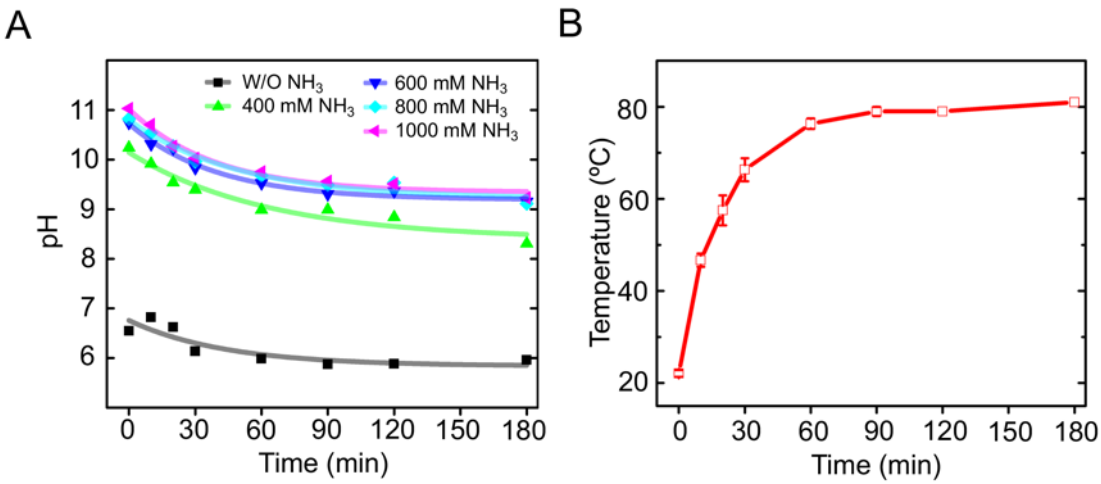

Figure 2-4 pH value and temperature of growth solution over time.

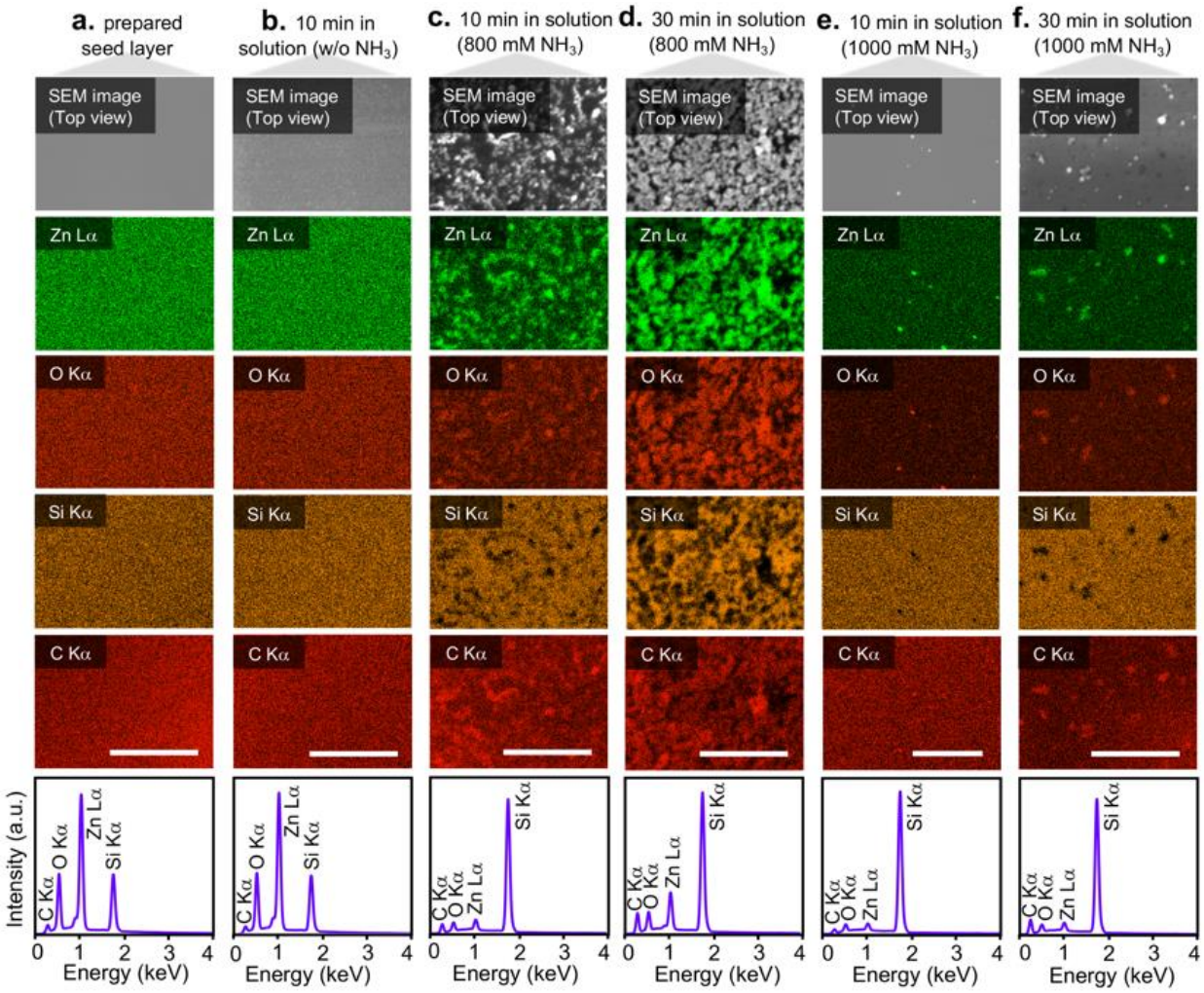

Figure 2-5 EDS mapping analysis of seed layer on silicon substrate after immersing into growth solution with varied ammonia concentration for 10 and 30 min, respectively (a, b, c, d, f scale bar = 1 μm; e scale bar = 5 μm).

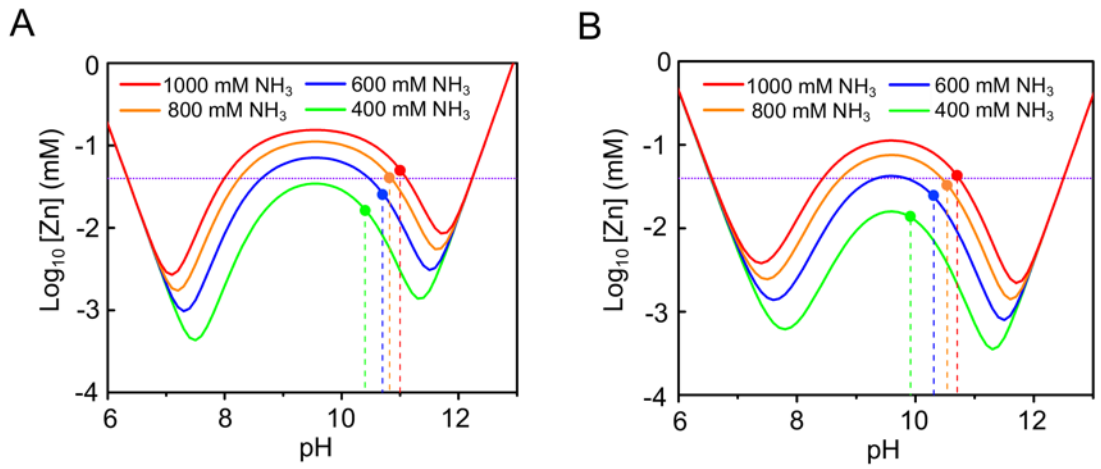

Figure 2-6. pH value dependent theoretical solubility of Zn(II) in aqueous solutions with varied concentrations of ammonia. **A.** pH value dependent theoretical solubility of Zn(II) in aqueous solutions with varied concentrations of ammonia at 25 ºC. **B.** pH value dependent theoretical solubility of Zn(II) in aqueous solutions with varied concentrations of ammonia at 60 ºC. Intersection points of solid curve and dash line in the same color represent theoretical solubility of Zn(II) at corresponding measured pH values. Horizontal dotted line represents Zn(II) concentration in prepared aqueous solution, which equals to zinc nitrate hexahydrate concentration, 40 mM.

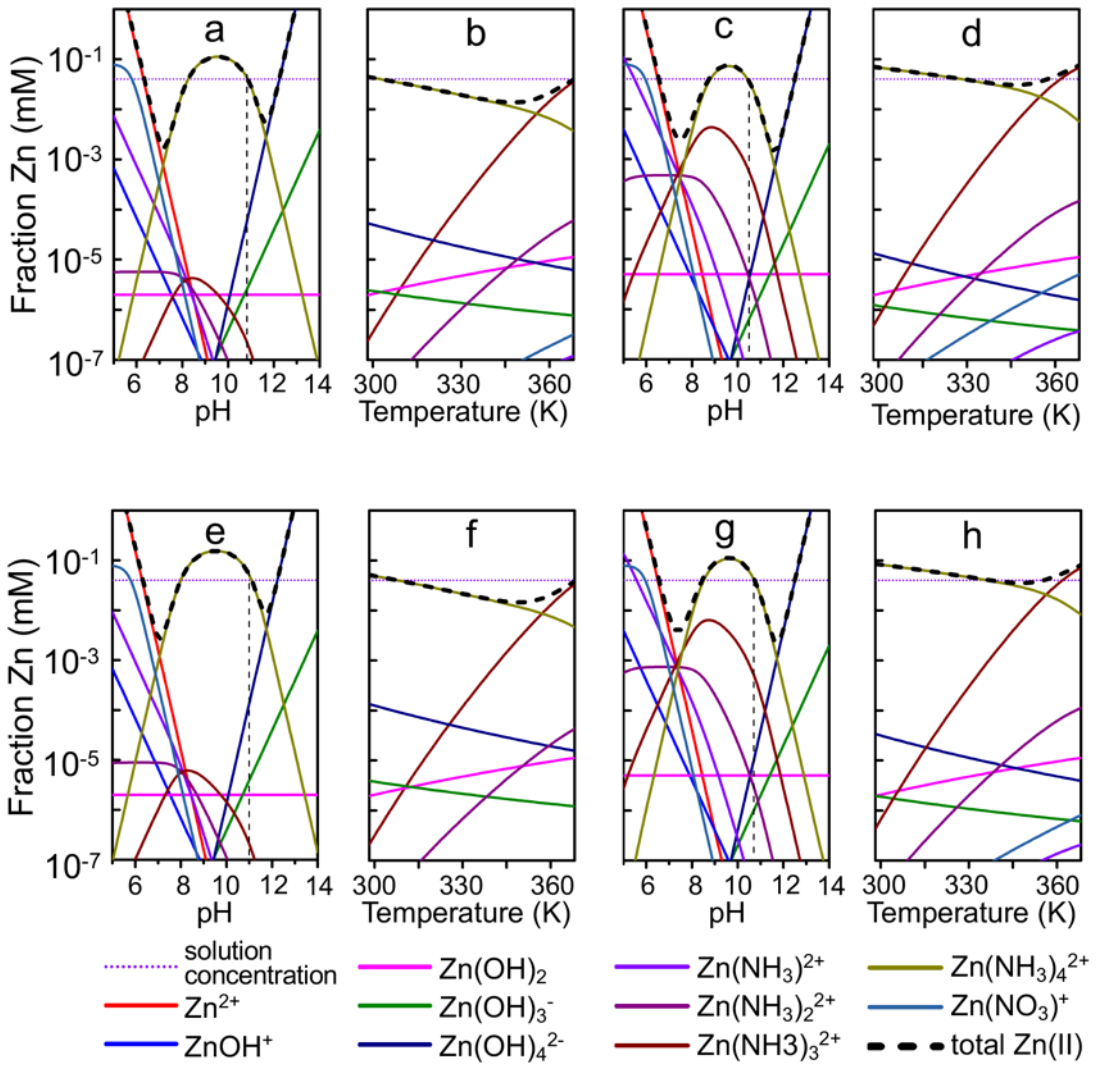

Figure 2-7 Speciation of dissolved Zn(II) versus pH and temperature in growth solution. **a**. Solution with 800 mM ammonia, 25 ºC (298 K). **b**. Solution with 800 mM ammonia, pH 10.8 (measured value at 25 ºC). **c**. Solution with 800 mM ammonia, 60 ºC (333 K). **d**. Solution with 800 mM ammonia, pH 10.5 (measured value at 60 ºC). **e**. Solution with 1000 mM ammonia, 25 ºC (298 K). **f**. Solution with 1000 mM ammonia, pH 11.0 (measured value at 25 ºC). **g**. Solution with 1000 mM ammonia, 60 ºC (333 K). **h**. Solution with 1000 mM ammonia, pH 10.7 (measured value at 60 ºC). Vertical dash line in a, c, e and g are measureed pH value.

CHAPTER III

Photolithographically Constructed Single ZnO Nanowire Device and Its Ultraviolet Photoresponse

In chapter III**,** sparse ZnO nanowire array with aspect ratio of ca. 120 and growth rate of 1 μm/h was synthesized by controlling density of seeds at initial stage of nanowire growth. The spatially-separated nanowires were cut off from growth substrate unbrokenly, and thus facilitate to construct a single-nanowire device by photolithography. The device exhibited a linear current-voltage characteristic associated with ohmic contact between ZnO nanowire and electrodes. The device further demonstrated reliable photoresponse with an I_{UV}/I_{dark} of ~100 to ultraviolet light irradiation.

Photolithographically Constructed Single ZnO Nanowire Device and Its Ultraviolet Photoresponse

3.1 Introduction

Single zinc oxide (ZnO) nanowire devices have been widely produced not only for use in research about intrinsic properties of ZnO at confined nanospace, but also for application in light-emitting diodes, photodetectors, and bio- and gas-sensors [1-6]. In general, the devices require high aspect ratio nanowires and use of costly electron beam (EB) lithography apparatuses, which present challenges for some researchers fabricating single nanowire devices [7, 8]. For the first challenge, although metal–organic chemical vapor deposition (MOCVD) can yield high aspect ratio ZnO nanowires [9, 10], the severe experimental conditions, and high apparatus cost prevent it from being widely adopted. For less hazardous synthesis, flexible control by nutrient solution composition, and low cost, researchers generally select hydrothermal synthesis to produce ZnO nanowires [11, 12]. In the hydrothermal synthesis, typical approaches to increase the aspect ratio of ZnO nanowires are, 1) adding polyethylenimine (PEI) to the growth solution to inhibit nanowire radial extension and prolong growth time [13, 14], or 2) adding $NH_3 \cdot H_2O$ to promote nanowire axial growth and a PEI to inhibit radial extension [15, 16]. For these two approaches, the former is bound by its slow growth rate, and the latter suffers from serious fusion at the bottom part of nanowires. For the second challenge of single nanowire device fabrication by transferring a single nanowire to a predefined location, single nanowire

devices can be practically fabricated by photolithography [17], but the complicated operation of picking up and transferring a single nanowire has to be implemented.

In the current work, we demonstrate a facile technique to hydrothermally synthesize a sparse ZnO nanowire array with high aspect ratio by suppressing the fusion at the bottom of nanowires. The fabricated nanowires were cut off from the growth substrate without breaking. A single-nanowire device was constructed via photolithography technique equipped with a micrometer control stage, instead of conventional EB lithography. Using the single-nanowire device, we characterized the electrical conduction properties of ZnO nanowires as well as their photoresponse to ultraviolet (UV) light irradiation.

3.2 Experimental

3.2.1 Growth and characterization of nanowires

Silicon substrates (N type) with a size of 20 mm × 10 mm × 0.625 mm were cleaned by heating them in a mixture of 98 % concentrated sulfuric acid and 35 % hydrogen peroxide (3 : 1 by volume) at 180 °C for 2 h, and then washing them with ultrapure water and blowing them dry with a nitrogen gas flow. Radio frequency sputtering was used to prepare a 50 nm thick ZnO seed layer on the clean substrates. Next, the substrates were immersed into 50 mL nutrient solution in individual Teflon cups containing 50 mM equimolar of zinc nitrate hexahydrate and hexamethylenetetramine. Ammonia concentration was adjusted to 800 mM by adding 25 % commercial ammonia solution. Then, 2 mM PEI (branched, low molecular weight, Aldrich) was added to the nutrient solution as a nanowire radial growth inhibitor, to result in a decreased nanowire areal density. The Teflon cups were covered with glass dishes and they were put into an oven, preheated to 95 °C, and left for 3 h. After 3 h, the substrates were immersed into fresh solution in order to obtain long wire arrays;

this was repeated 10 times (total immersion time of 30 h). In this way we were able to synthesize a 30 μm length nanowire array on each substrate in 30 h. Finally, the samples were washed with ultrapure water and acetone, before being dried on an 80 °C hot plate for 10 min. We imaged the fabricated nanowires using a scanning electron microscope (SEM; Zeiss Supra 40 VP).

3.2.2 Device fabrication

The nanowires were cut from the substrates by a scalpel and suspended in isopropanol. The suspension was dropped onto a 20 mm× 20 mm SiO_2/Si substrate using a micropipette and dried in air. A layer of hexamethyldisilazane as tackifier was spin coated on the dried substrate with the nanowires at 3000 rpm for 8 s, and then this was covered with photoresist AZ 5200-E (purchased from Tokyo Ohka Kogyo) by spin coating at 1000 rpm for 120 s. Suitable nanowires were selected and they were exposed for the electrode pattern using photolithography equipment (Model DDB-700, Neoark Corporation). After pattern development, sputter-deposited electrodes were obtained that consisted of layers of Ti (10 nm), Pt (50 nm) and Au (100 nm).

3.2.3 Measurement of electrical resistivity

We measured resistance of the ZnO nanowires by the four probes measurement. A source meter (Model 2401, Keithly) was connected to two outer electrodes to provide the voltage and measure the current in circuit. A digital multimeter (34461A, Keysight) was connected to two inner electrodes and used for component voltage measurement. In photoresponse detection, the source meter was connected to two inner electrodes to provide a voltage and measure the current. A handheld UV lamp with wavelength of 365 nm (0.29 mW/cm^2) was used to illuminate the devices. The measurement was carried out in the dark in air.

3.3 Result and Discussion

Research studies have shown that a certain amount of PEI hinders lateral growth of ZnO nanowires in solution [13-16]. In the current work, we carried out ammonia-assisted seed engineering with PEI as cation surfactant to control density of the seeds, realizing synthesized sparse nanowire arrays with ~120 aspect ratio at a 1 μm/h growth rate. According to the SEM images in Fig. 3-1A, it is clear that the areal density of the nanowires gradually decreases with the increased amount of added PEI. The statistical analysis in Fig. 3-1B confirms the inverse trend between nanowire areal density and the added PEI weight. This indicates that PEI plays a significant role on suppressing the initial nucleation. The statistical results in Fig. 3-1C demonstrate a small quantity of PEI has almost no effect on nanowire diameter and growth rate. We were able to boost the nanowire growth rate from 0.3 - 0.5 μm/h in typical experiments [15, 16], to 1 μm/h and produce an ultralong sparse ZnO nanowire array with ~120 aspect ratio. What is more, because of the low areal density, the serious fusion phenomenon of nanowires in the bottom part of the array is almost completely avoided (shades of light red in Fig. 1A). As shown in Fig.3-1D, the fusion length proportion in total length gradually decreases with the increase of added PEI amount. The decrease of this proportion means that nanowires keep enough length for device fabrication after they are cut from the substrate.

According to XRD spectra of ZnO (JCPDS Card No. 36-1451), typical crystallographic peaks of ZnO nanowires (2 mM PEI, 27 h growth, ~ 30 μm length) are clearly seen in the XRD patterns (Fig. 3-2A). A significant increase of (002) peak intensity is measured after annealing nanowires at 600 °C in vacuum for 2 h. The preferential nanowires growth orientation of [001] direction and improvement of crystallinity after

annealing explain the prominent increase of (002) peak. The room temperature photoluminescence (PL) spectra and multiple Gaussian peak fitting (inset shows the fitting result of annealed ZnO nanowires) of green-yellow (~565 nm) and yellow-orange (~620 nm) defect emission in as-grown and annealed ZnO nanowires are shown in Fig. 3-2B. The dominant defect emission changes from green-yellow to yellow-orange after annealing, indicating the reduction and the reconstruction of ZnO crystal in nanowires. We consider the redshift of defect emission by decomposition of the possible presence of $Zn(OH)_2$ on the nanowire surface [18], and the involvement of interstitial oxygen [19]. The bond breaking of the interstitial oxygen is supposed weaken defect emission [20]. An intensity reduction and a redshift of the broad defect peak observed after heat treatment at 600 °C in vacuum indicate a decrease in the point defect concentration and enhancement of crystallinity.

After obtaining ultralong nanowires, we employed a photolithography method to obtain single nanowire devices. The fabrication procedure is described in the experimental section and is as shown in Figure 3-3A. Figure 3-3B intuitively presents nanowires cut from the substrate and deposited on a SiO_2/Si substrate using a micropipette, followed by drying it naturally in air. From the SEM image of the fabricated device shown in Fig. 3-3C, we can see that a four-terminal single nanowire device was neatly bridged between a 5 μm gap electrodes. Here, we carry out photolithography instead of electron beam irradiation to realize the structure of our single nanowire devices. The simpler procedures and less costly equipment will encourage more researchers to examine the electrical and optical properties of nanowires.

For a characterization of the nanowire electrical property, we measured electrical resistivity of the nanowire by the four probe sensing method (Fig. 3-4A). Figure 3-4B presents the I-V characteristics of the nanowires; we see that linear behaviors were achieved between [-0.25 V, +0.25 V]. The result demonstrates that good ohmic contacts between nanowires and metal electrodes have been realized. We estimated nanowire resistivities by Ohm's law based on the measurement of nanowire diameters and channel lengths between the inner two electrodes. Existence of the shallow energy level defects suggest that possibly the oxygen vacancy or the Zn interstitial defects result in an effective enhancement of electrical conductivity. The calculated resistivities vary in a range from 2.8 to 26.9 Ω·cm, which are comparable with previous studies [21]. To characterize the nanowire photoconductive properties, electrical measurements were performed in the states of UV light on and UV light off. Figure 3-4C compares the current-voltage (I-V) curves measured on a device with 5 μm length nanowire channel. Results show that, without UV illumination, the detected average resistance is above 15.1 MΩ and that indicates the nanowire is highly insulated in the dark; while when the device is exposed to UV light, the nanowire resistance is 1.9 MΩ, and that is a decrease by almost 1 order of magnitude. What is more, no matter with or without UV light irradiation, the current-voltage curves exhibit quite good linear behavior. The characteristics of the photoconductive ZnO nanowire suggest that it is a good candidate for a UV photodetector. Figure 3-4D shows the photoresponse to UV light being turned on and off as a function of time. Significant differences of the detected current clearly indicate that the fabricated UV detector can be reversibly switched between the low (dark) and the high (UV) conductivity states. With 1 V bias, our UV detector exhibits a ~100 (I_{UV} / I_{dark}) sensitivity, 23 s response

time and 70 s recovery time. The photoconductive nanowire seems to be a good candidate for highly sensitive UV light detectors, and chemical or biological sensors when combined with suitable surface modification.

3.4 Conclusion

In summary, we successfully suppressed the fusion of nanowires at their bottom part and promoted nanowire growth rate to 1 μm/h by ammonia-assisted seed engineering and PEI as cation surfactant to control areal density of the seeds. With ~120 aspect ratio, nanowires were used to fabricate single-nanowire devices by a manageable photolithography apparatus. We estimated nanowire resistivities to be in the range of 2.8 to 26.9 Ω·cm due to ohmic contacts between the single nanowire and metal electrodes. The device exhibited a ~100 (I_{UV} / I_{dark}) sensitivity on exposure to UV irradiation, which enabled it to serve as UV light detector or switching device.

3.5 References

[1] D. Kalblein, H. Ryu, F. Ante, B. Fenk, K. Hahn, K. Kern, and H. Klauk, *ACS Nano*, **2014**, *8*, 6840

[2] J. Bao, M. A. Zimmler, and F. Capasso, *Nano Lett.*, **2006**, *6*, 1719

[3] L. Zhang, Y. Wang, H. Wu, M. Hou, J. Wang, L. Zhang, C. Liao, S. Liu, and Y. Wang, *Nanoscale*, **2019**, *11*, 8319

[4] E. Danielson, V. Dhamodharan, A. Porkovich, P. Kumar, N. Jian, Z. Ziadi, P. Grammatikopoulos, V. A. Sontakke, Y. Yokobayashi, and M. Sowwan, *Sci. Rep.*, **2019**, *9*, 17370

[5] A. Choi, K. Kim, H.-I Jung, and S. Y. Lee, *Sens. Actuators B Chem.*, **2010**, *148*, 577

[6] Y. Hu, J. Zhou, P.-H. Yeh, Z. Li, T.-Y. Wei, and Z. L. Wang , *Adv. Mater.*, **2010**, *22*, 3327

[7] L. Oleg, C. Vasilii, P. Vasile, A. Mahdi, B. R. Beatriz, C. Lee, T. Ion, V. Bruno, P. Thierry, and A. Rainer, *Sens. Actuators B Chem.*, **2016**, *223*, 893

[8] A. Choi, K. Kim, H. Jung, and S. Y. Lee, *Sens. Actuators B Chem.*, **2010**, *148*, 577.

[9] L. Hu, Q. Liao, Z. Xu, J. Yuan, Y. Ke, Y. Zhang, W. Zhang, G. P. Wang, S. Ruan, Y.-J. Zeng, and S.-T. Han, *ACS Photon.*, **2019**, *6*, 886

[10] T. Lim, J Bong, E. M. Mills, S. Kim, and S. Ju, *ACS Appl. Mater. Interfaces*, **2015**, *7*, 16296

[11] J. Joo, B. Y. Chow, M. Prakash, E. S. Boyden, and J. M. Jacobson, *Nat. Mater.*, **2011**, *10*, 596

[12] S. Xu and Z. L. Wang, *Nano Res.*, **2011**, *4*, 1013

[13] J. Qiu, X. Li, F. Zhuge, X. Gan, X. Gao, W He, S.-J. Park, H.-K. Kim, and Y.-H. Hwang, *Nanotechnology*, **2011**, *21*, 195602

[14] L.-Y. Chen, Y.-T. Yin, C.-H. Chen, and J.-W. Chiou, *J. Phys. Chem. C*, **2011**, *115*, 20913

[15] M. Law, L. E. Greene, J. C. Johnson, R. Saykally, and P. Yang, *Nat. Mater.*, **2005**, *4*, 455

[16] C. Xu, P. Shin, L. Cao, and D. Gao, *J. Phys. Chem. C*, **2010,** *114*, 125

[17] Q. Li, S.-M. Koo, C. A. Richter, M. D. Edelstein, J. E. Bonevich, J. J. Kopanski, J. S. Suehle, and E. M. Vogel, *IEEE Trans. Nanotechnol.*, **2007**, *6*, 256

[18] H. Zhou, H. Alves, D. M. Hofmann, W. Kriegseis, B. K. Meyer, G. Kaczmarczyk, and A. Hoffmann, *Appl. Phys. Lett.*, **2002**, *80*, 210

[19] F. Han, S. Yang, W. Jing, K. Jiang, Z. Jiang, H. Liu, and L. Li, *Opt. Express*, **2014**, *22*, 11437

[20] L. E. Greene, M. Law, J. Goldberger, F. Kim, J. C. Johnson, Y. Zhang, R. J. Saykally, and P. Yang, *Angew. Chem. Int. Ed.,* **2003**, *42*, 3031

[21] W. Geng, S Kostcheev, C. Sartel, V. Sallet, M. Molinari, O. Simonetti, G. Lérondel, L. Giraudet, and C. Couteau, *Phys. Status Solidi (C)*, **2013**, *10*, 1292

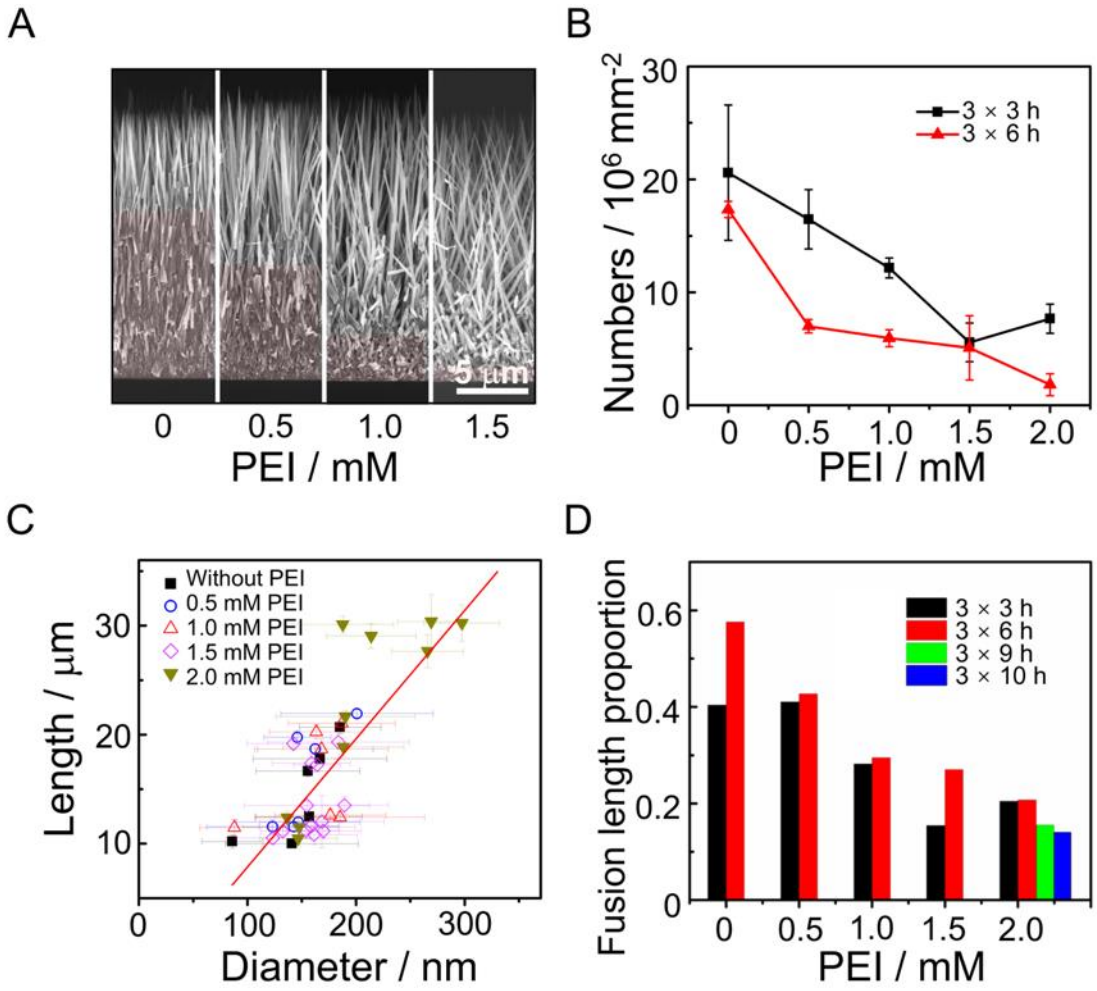

Fig. 3-1 Morphology analysis of ZnO nanowires. **A**. SEM images of ZnO nanowires grown in nutrient solutions containing 800 mM ammonia and various weights of added PEI. **B**. Numbers of nanowires in a unit area. **C**. Nanowire diameter vs. its length for different weights of added PEI. The red line is a linear fit to the statistical data, and the error bars represent the standard deviation. **D**. The proportion of bottom fusion length in the total length of the nanowires for different weights of added PEI.

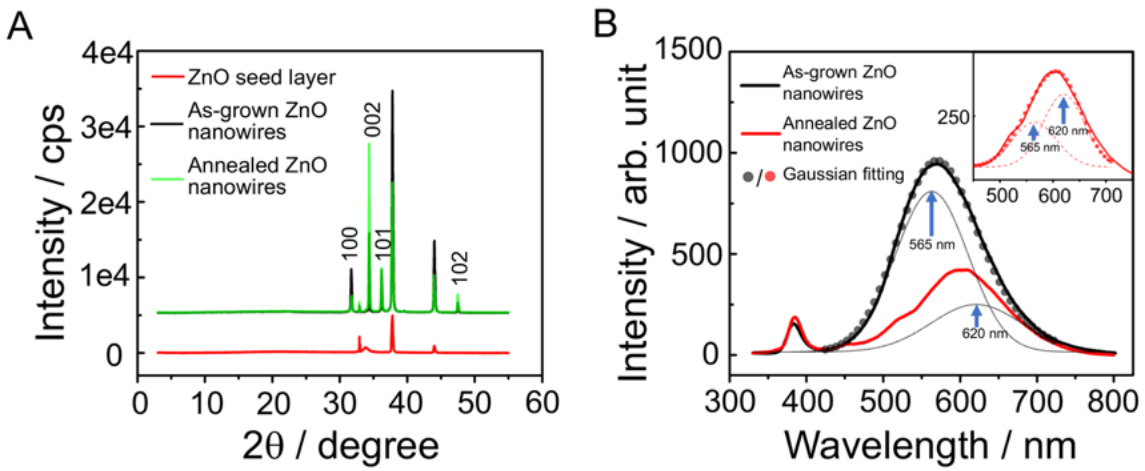

Fig. 3-2 Characterization of ZnO nanowires. **A**. XRD patterns of ZnO nanowires and Si substrate with sputtered ZnO seed layer. Peaks with numbers on them indicate typical peaks for wurtzite characteristics. **B**. Room temperature photoluminescence spectra of ZnO nanowires.

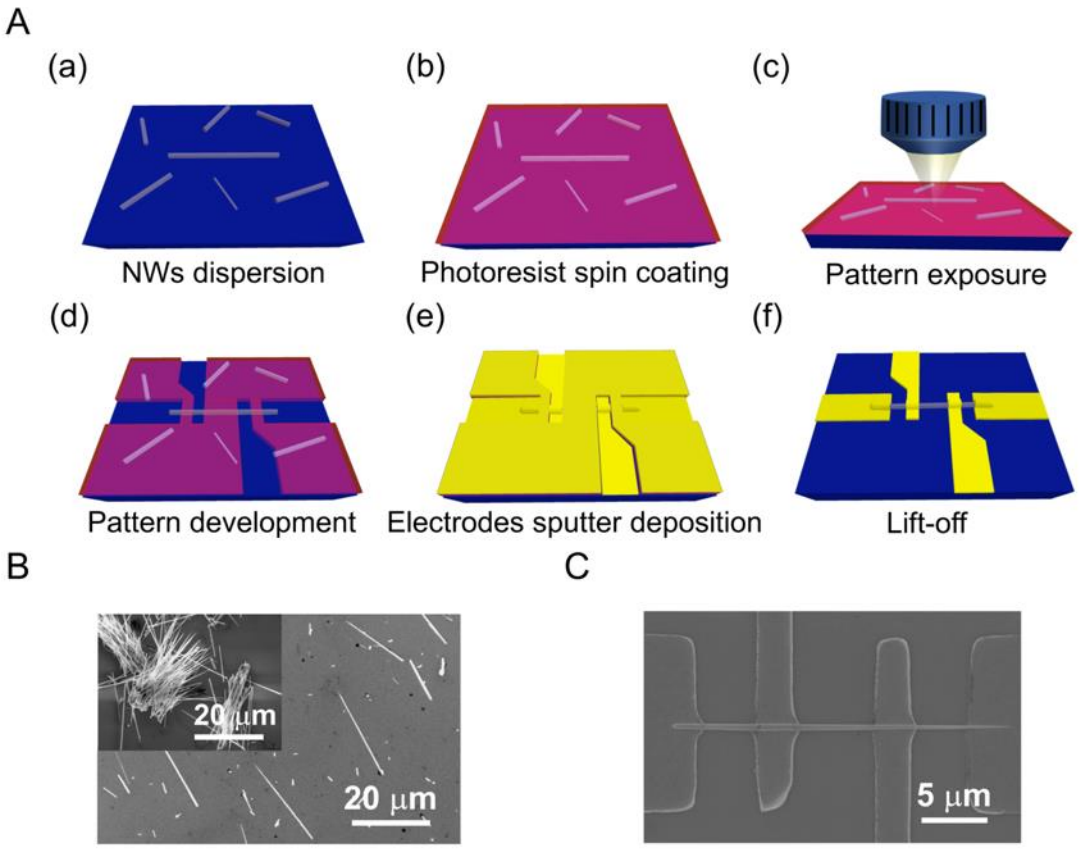

Fig. 3-3 Schematic drawings of the fabrication of the single nanowire device and SEM images of the device. **A**. Schematic drawings of the fabrication. **(a)**. Applying a suspension containing nanowires to a substrate followed by drying. **(b)**. Covering with photoresist. **(c)**. Selecting the suitable nanowires, and exposing the pattern. **(d)**. Developing the pattern. **(e)**. Sputter-depositing the metal electrodes. **(f)**. Lifting-off excess photoresist and metal layer. **B**. SEM image of ZnO nanowires cut from the substrate before (inset) and after 2 s ultrasonic dispersion. **C**. SEM image of the single nanowire device. Distance between two adjacent electrodes was 5 μm.

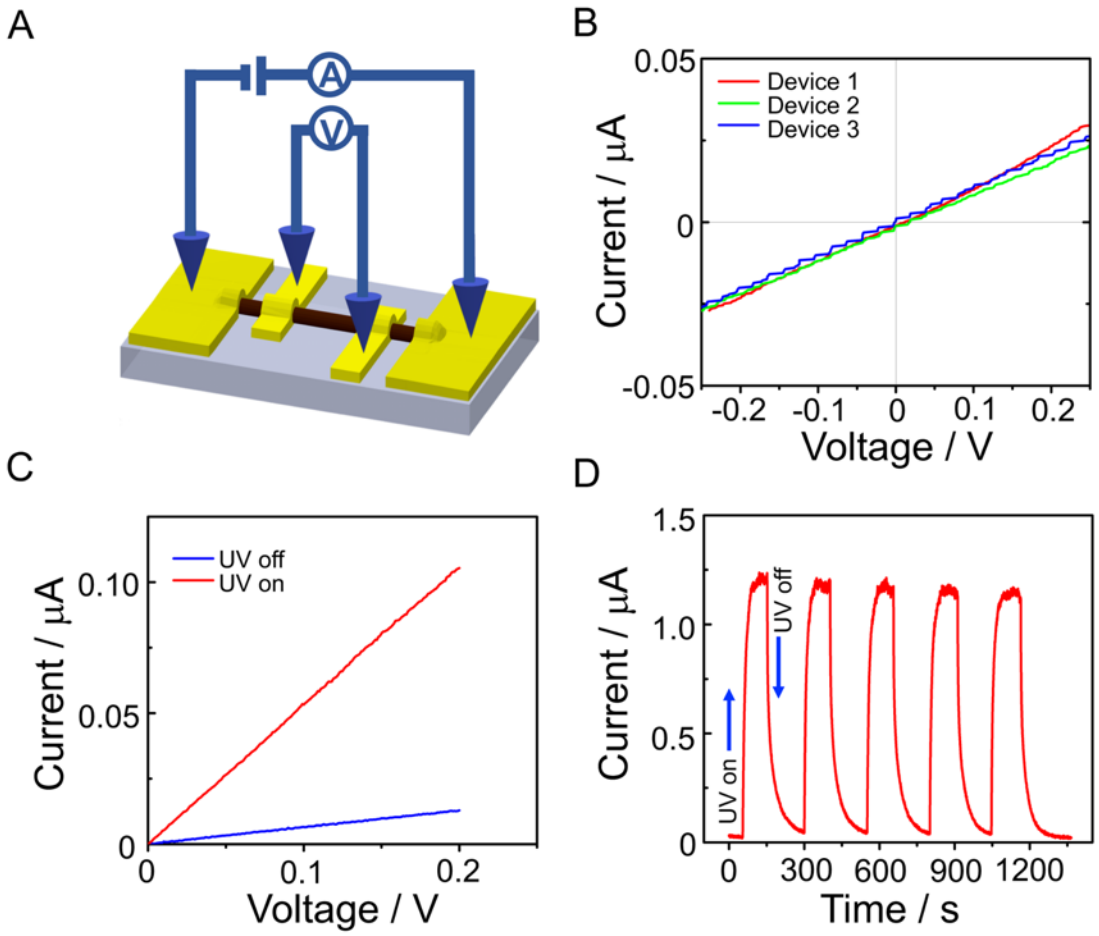

Fig. 3-4 Schematic of the four-probe sensing method and device photoelectric properties. **A**. Schematic of the four-probe sensing method. Partial voltage between the two inner electrodes was measured by a digital multimeter. A source meter was used to apply the voltage and measure current. **B**. Current-voltage (I-V) curves of several devices. **C**. I-V curves of dark current (blue) and photocurrent (red) of a single ZnO nanowire device under UV illumination. **D**. Device photo response to UV light being turned on and off, the bias on the nanowire is 1 V.

CHAPTER IV

Thermal Annealing Derived Stabilization of Metal Oxide Core-shell Nanowire Towards Sensing Response to miRNA 21

In chapter IV, atomic layer deposition (ALD) technology boosted constructure of ZnO/ Al2O3, ZnO/ SnO_2, and ZnO/ NiO core-shell nanowires. Nanodevices embedding the core-shell nanowires were responded to miRNA 21 in aqueous environment. Metal oxide composites are structured to passivate ZnO nanowire surface. Thermal treatment improved nanowires crystallinity, and also optimized the nano-heterostructure. These two effects further increased the stability of nanowire, and enhanced sensing response of the sensors. Comparison of different response signal, a hypothesis was presented to further understand the sensing mechanism between metal oxide surface and miRNA. Based on a mature research of core-shell nanodevices, the selective fingerprinting of miRNAs by material-dependent nanosensors arrays is expected to realize.

Thermal Annealing Derived Stabilization of Metal Oxide Core-shell Nanowire Towards Sensing Response To miRNA 21

4.1 Introduction

Semiconducting metal oxide nanowires possess unique physical properties and flexible manufacture, have been treat as a popular candidate embedded in various devices [1, 2]. In the last two decades, application of these devices has been extended to the field of photoelectric [3], energy conversion [4–6] and physical/chemical sensing [7–9]. With the increase demand of environment monitoring, microscopic reaction mechanism exploration, self-health management, and medical diagnosis, individual metal oxides nanowire devices as bio/chemical sensors exhibit enormous potential due to their high-sensitivity, selectivity, easy integration, and miniaturization [10–13]. However, there are still unexpected challenges need to be overcome, for example the thermal tolerance and negative effects of humidity limit the service life and sensitivity for gas sensors [7, 14, 15]; the chemical stability and undifferentiated response(realization of selective response always by virtue of complex specific modification) severely limit the application of resistive-type chemical sensors in aqueous condition [16–18]. Recent researches suggest that the involve of composite metal oxide may qualify for enhancing stability and improving sensing performance of the individual nanowire devices to a certain extent [19,20]. Active metal oxide nanowires (ZnO, for instance) covered with a more stability metal oxide layer evidently exhibit enhanced stability no matter in harsh thermal environment but also in aqueous condition [1, 21–25]. As for the improvement of sensors performance, researchers attribute to the formation of a heterojunction between the two kinds of metal oxides. Derek

R. Miller et. al. summary the effects of the heterojunction on gas sensing in three aspects: 1) electronic effects, mainly including Fermi level equilibration-induced band bending and depletion layer formation; 2) chemical effects, mainly including synergistic surface reaction and decrease in activation energy; and 3) geometrical effects, mainly including surface area enhancement and grain refinement [19]. Comparing with the gas sensor, although with a deposition of stable metal oxide shell, a nano-heterostructure sensor remain difficulty to maintains integrity in aqueous condition. Different from the gas sensor which sensing response is resultant of a shift on equilibrium of the surface chemisorbed oxygen reaction and a target gas [7, 26], an interaction between the charged surface and target molecules or ions is the response signal source for a metal oxide-based sensor in aqueous condition [27–29]. The hydration of metal oxide nanowire embedded sensor in an aqueous environment caused by chemisorption of water leading to a surface hydroxide of nanowire. A charged surface is produced by further protonation or deprotonation of the surface hydroxide, and is governed by given pH value of solution [25, 27]. Besides mention above, coordination between composition metal on nanowire surface and analytes (treated as ligands) in solution is also a response signal source [30, 31]. Therefore, a nano-heterostructure embedded sensor enhances its sensing response not only based on the mechanism mentioned above, but also can be realized by depositing an appropriate metal oxide shell. Recently, ZnO possesses the advantages of non-toxicity, good biocompatibility, and flexible synthesis processes, has been used in various bio/chemical sensor developments. However, it is remained that the dissociation of nanoscale ZnO in aqueous environment cannot be ignored. Although with bio-modification, ZnO surface to obtain a sustained specific response need to be improved urgently.

Here, atomic layer deposition (ALD) technology boosted constructure of ZnO/NiO, ZnO/SnO_2, and ZnO/Al_2O_3 core-shell nanowires. ALD technology allows for accuracy controlling of shell deposition speed and thickness, creating high quality nano-heterostructure to improve sensor performance. Nanodevices embedding the core-shell nanowires were responded to miRNA 21 in aqueous environment. Thermal annealing was implemented to improve nanowires stability in aqueous environment. Formation of core-shell nanostructures, on the one hand, thermal annealing caused diffusion of deposited metal oxide layer on ZnO nanowire surface increased stability of nanowire. On the other hand, enhanced the electrical response of ZnO nanowire to biomolecular potentially. Comparison of response among nanodevices with different typed of deposited metal oxide layer assisted to reveal the response mechanism. A mature research achievement on core-shell nanodevices is expected to realize structure nanodevices array towards specific, high-sensitive fingerprinting of miRNAs.

4.2 Experimental

4.2.1 Growth of ZnO nanowires

Silicon substrates (N type) with a size of 20 mm × 10 mm × 0.625 mm were cleaned by heating them in a mixture of 98 % concentrated sulfuric acid and 35 % hydrogen peroxide (3 : 1 by volume) at 180 °C for 2 h, and then washing them with ultrapure water and blowing them dry with a nitrogen gas flow. Radio frequency sputtering was used to prepare a 50 nm thick ZnO seed layer on the clean substrates. Next, the substrates were immersed into 50 mL nutrient solution in individual Teflon cups containing 50 mM equimolar of zinc nitrate hexahydrate and hexamethylenetetramine. Ammonia concentration was adjusted to 800 mM by adding 25 % commercial ammonia solution. Then, 2 mM PEI (branched, low

molecular weight, Aldrich) was added to the nutrient solution as a nanowire radial growth inhibitor, to result in a decreased nanowire areal density. The Teflon cups were covered with glass dishes and they were put into an oven, preheated to 95 °C, and left for 3 h. After 3 h, the substrates were immersed into fresh solution in order to obtain long wire arrays; this was repeated 10 times (total immersion time of 30 h). In this way we were able to synthesize a 30 μm length nanowire array on each substrate in 30 h. Finally, the samples were washed with ultrapure water and acetone, before being dried on an 80 °C hot plate for 10 min. We imaged the fabricated nanowires using a scanning electron microscope (SEM; Zeiss Supra 40 VP).

4.2.2 Core-shell nanostructures fabrication

Before fabrication of the metal oxides layer by ALD, the as -grown ZnO nanowires array was cleaned in a UV Ozone Cleaner (UV-1 model, Samco Inc., Japan) for 60 seconds. The cleaned nanowires array was put into ALD (Savannah, Cambridge Nano Tech Ltd., USA) chamber immediately, deposition of metal oxide shell was implemented. The precursors used in our experiment are diethylzinc for ZnO, bis(ehtylcyclopentadienyl) nickel for NiO, tetrakis(dimethylamido) tin for SnO_2, and trimethylaluminum for Al_2O_3, respectively. A 3 nm thickness metal oxide shell was fabricated at last. All of the precursors are purchased from Japan Advanced Chemicals Ltd., Japan. Detail about the deposition recipes is listed in Table.4-1. For the process of thermal treatment, core-shell nanowires array was put into an oven at 450 °C for 1 hour in ambient environment. After cooling down to room temperature, the core-shell nanowires were dispersed and suspended in isopropanol by 10 seconds ultrasonic processing. The suspension can be stored in a short period (less than two weeks).

Table 4-1 ALD condition of metal oxides shell

Parameter / Material	Precursor 1	Precursor 2	Deposition mode	Precursor 1 preheat temperature	Growth temperature	Pulse time of precursor 1	Cycles
ZnO	diethylzinc	H_2O	Exposure	W/O	150 °C	0.015 s	15
NiO	bis(ehtylcyclopentadienyl) nickel	O_3	Exposure	95 °C	250 °C	1 s	200
SnO_2	tetrakis(dimethy-lamido) tin	H_2O	Exposure	60 °C	150 °C	0.5 s	50
Al_2O_3	Trimethylalumi-num	H_2O	Exposure	W/O	150 °C	0.015 s	20

4.2.3 Individual core-shell nanowire device fabrication

Figure 4-2 shows flowchart of individual nanowire device fabrication by EB. A brief description of the flowchart is described as follows: After fabrication of outer part of electrodes on the 20 mm× 20 mm Si/SiO_2 (525 ± 25 μm with100 nm thickness SiO_2, purchased from Electronics and Materials Corp. Ltd., Japan) substrate, the suspension was dropped onto the substrate using a micropipette and dried in air. The relative position of nanowires are confirmed by microscopy or SEM. Then, the substrate covered a layer of photoresist ZEP-520A (purchased from Tokyo Ohka Kogyo) by spin coating at 3000 rpm for 120 s. Accurate exposure of the inner part electrodes pattern was carried out suing using Electron Beam Lithogrophy instrument (Elionix Corporation, Japan). After pattern development, sputter-deposited electrodes were obtained that consisted of layers of Ti (10 nm), Pt (100 nm). Next, a layer of PMMA was coated onto the substrate at 3000 rpm for 120 s. A sensing window was developed based on EB accurate exposure. This sensing window only let the nanowire exposure to sensing environment, and protects the electrodes from there.

4.3 Result and Discussion

As shown in figure 4-1, we used the thermal annealing derived stabilization of metal oxide core-shell nanowire towards sensing response to miRNA 21. Nanodevices in constant chemical/bio target sensing, chronic in vivo cell-recording, implantable tissues, and some other physiological surroundings, require long-term stability. However, pristine ZnO nanowire dissociated easily with the changes of environment, such as solution pH value, salt concentration, ion species, and temperature. In our design, a 3 nm thickness metal oxide shell is deposited on ZnO surface to form a nano-heterostructure. The composite metal oxides protect ZnO nanowire from contacting with solution directly. Devices sensing response is expected to be enhanced by nano-heterostructure, and appropriate metal oxides could be selected to manage the surface charge of nanowire increasing sensing selectivity. ZnO nanowires are prepared via the low-temperature hydrothermal procedure, various defect states generate during NW growth process inevitably because of their relatively low formation energy. In sensing applications, some of defect states in ZnO NWs act as the charge recombination centers of the sensing device. Reducing the defect-state densities of ZnO NWs plays a key role in improving crystallinity, enhancing stability, inhibiting charge recombination and in turn improving the performance of sensors. In our case, a thermal treatment is implemented to improve nanowire crystallinity, clean the interface of metal oxides composites. As a result, the stability of our devices would be further increased. An enhancement of sensitivity is expected depend on creating more intimate electrical contact at the interface. The individual nanowire device is fabricated as the flowchart shown in Figure 4-2. It is noted that the electrodes are protected by covering a layer of PMMA, only remain the core-shell

nanowire contacting with the aqueous solution. To facilitate measurement, a PDMS groove is bonding to PMMA layer above the sensing window (show in Figure 4-2 j).

In our experimental design, ZnO, NiO, SnO_2, and Al_2O_3 are selected as shell metal oxides, in which, ZnO is treated as control, NiO is a p-type semiconductor, SnO_2 and Al_2O_3 with high stability in aqueous environment. Figure 4-3 shows the current-voltage (I-V) curves of the core shell embedded devices. The embedded nanowires all with an ultrathin metal oxides layer fabricated by ALD. We set the thickness of the metal oxides layer at around 3 nm. From the figure, conductivity of NiO, SnO_2 covered nanowires decreased, the nanostructure with Al_2O_3 layer shows no current. Reduction of conductivity is attribute to the present of metal oxides layer between ZnO nanowire and metal electrodes. The state of Al_2O_3, can be interpreted as the insulation of Al_2O_3. According to figure 4-4 A, core-shell nanowires are embedded in devices, and measurement of devices current in water condition is carried out. Dramatic decreases of current to almost zero core-sell are observed in all three kinds of composites. After adding of water, ZnO/ZnO and ZnO/NiO maintain conductivity around 5 min; ZnO/SnO_2 shows longer time of conductivity, lasts for almost 15 min. ZnO/Al_2O_3 without data because of insulation. Although passivated by depositing of metal oxides shell, the almost zero current let us consider the broken of nanowires. What is more, the order of current plunges to zero is consistent with dissolution rate of corresponding metal oxide nanoparticles shown in figure 4-4 B (refer to [25]). SEM images in figure 4-4 C shows the status of nanowires. It is obvious that all nanowires are dissociated during measurement. For ZnO/ZnO and ZnO/NiO nanostructures, the serious dissociation lead to the result of breakage. For the case of ZnO/SnO_2, the dissociation

produces a rough surface, causing current fluctuations along with time extension (shown in figure 4-4 A).

Next, we implement the measurement of individual nanowire devices fabricated with core-shell nanowire after thermal treatment in air 450 ^{o}C for 1 hour. The injection of oxygen reduces the oxygen vacancies (as show in figure 4-5 B) enhancing the crystallinity of nanostructure. The heat also decomposes and desorb the chemical substances on composites interface. These two effects are considered increasing stability of nanomaterials and enhancing the sensing response. From figure 4-5 A, ZnO/NiO and ZnO/ZnO maintain integrity more than 15 min, much longer than without thermal treatment status. The annealing significantly improves the stability of metal oxides nanowires. What is more, ZnO/ Al_2O_3 nanowire changes into conductive, due to the thermal-induced metal atomic diffusion (a certain amount of zinc atoms diffuses to surface of nanowire, as shown in figure 4-5 C). As miRNA 21 is a proved important biomarker for cancers and inflammations (refer to [32], shown in figure 4-6 A), we select it to confirm the device performances. Measurement begins with cover the nanowire by water. After system stabilization, solution contains 10 μm miRNA 21 is added on sensing surface (schematic diagram shown in figure 4-6 B). Figure 4-6 C reveals the electrical response of core-shell nanowires to miRNA 21. Our results suggest that miRNA 21 can excite electrical response from all four kinds of nanowires. And the signals are enhanced after thermal treatment, besides in ZnO/NiO state. The reduction of response from ZnO/NiO can be explained by thermal-induced atom diffusion transfer n-pZnO-NiO abrupt junction to n-pZnO-NiO graded junction. It is interesting that ZnO/SnO_2 and ZnO/Al_2O_3 show an inverse result with ZnO/ZnO and ZnO/NiO when response to miRNA 21. This phenomenon can be further

interpreted in terms of different hydration between metal oxide surface and chemisorbed water. ZnO/ZnO and ZnO/NiO nanowires exhibit positive ζ-potential in the measurement condition, implying a protonation of water adsorbed on nanowire surface. On the contrary, ZnO/SnO_2 and ZnO/Al_2O_3 nanowires show negative ζ-potential in the measurement condition, a water deprotonation occurs on nanowire surface. Phosphate groups in miRNA 21 phosphate backbone are ionized in aqueous surrounding. In order to easily explain, we define the miRNA molecules ionization products as $[RNA\text{-}HPO_4]^-$ and $[RNA\text{-}PO_4]^{2-}$. For our ZnO/ZnO and ZnO/NiO-based device, interaction between nanowire surface and biomolecule is described as $M\text{-}OH_2^+ + [RNA\text{-}PO_4]^{2-} \rightarrow M\text{-}OH + [RNA\text{-}HPO_4]^-$ (M: Zn, Ni). Deprotonation of $M\text{-}OH_2^+$ increases carrier (for a n-type ZnO, the carrier is electron) density resulting in raising of nanowire conductivity. For our ZnO/SnO_2 and ZnO/Al_2O_3 cases, interaction between nanowire surface and biomolecule is described as $M\text{-}O^- + [RNA\text{-}HPO_4]^- \rightarrow M\text{-}OH + [RNA\text{-}PO_4]^{2-}$ (M: Sn, Al). Protonation of $M\text{-}O^-$ reduces carrier density in conductive channel resulting in a reduction of current.

4.4 Conclusion

Nanodevices embedding the core-shell nanowires were responded to miRNA 21 in aqueous environment. Metal oxide composites are structured to passivate ZnO nanowire surface. Thermal treatment improved nanowires crystallinity, and also optimized the nano-heterostructure. These two effects further increased the stability of nanowire, and enhanced sensing response of the sensors. Comparison of different response signal, a hypothesis was presented to further understand the sensing mechanism between metal oxide surface and

miRNA. Based on a mature research of core-shell nanodevices, the selective fingerprinting of miRNAs by material-dependent nanosensors arrays is expected to realize.

4.5 References

[1] Lien, D.-H.; Durán Retamal, J. R.; Ke, J.-J.; Kang, C.-F.; He, J.-H. Surface Effects in Metal Oxide-Based Nanodevices. *Nanoscale* **2015**, *7 (47)*, 19874–19884.

[2] Shen, G.; Chen, P.-C.; Ryu, K.; Zhou, C. Devices and Chemical Sensing Applications of Metal Oxide Nanowires. *J Mater Chem* **2009**, *19 (7)*, 828–839.

[3] Ouyang, W.; Teng, F.; He, J.-H.; Fang, X. Enhancing the Photoelectric Performance of Photodetectors Based on Metal Oxide Semiconductors by Charge-Carrier Engineering. *Adv. Funct. Mater.* **2019**, *29 (9)*, 1807672.

[4] He, J. H.; Hsin, C. L.; Liu, J.; Chen, L. J.; Wang, Z. L. Piezoelectric Gated Diode of a Single ZnO Nanowire. *Adv. Mater.* **2007**, *19 (6)*, 781–784.

[5] Law, M.; Greene, L. E.; Johnson, J. C.; Saykally, R.; Yang, P. Nanowire Dye-Sensitized Solar Cells. *Nat. Mater.* **2005**, *4 (6)*, 455–459.

[6] Patel, M.; Kim, H.-S.; Kim, J.; Yun, J.-H.; Kim, S. J.; Choi, E. H.; Park, H.-H. Excitonic Metal Oxide Heterojunction (NiO/ZnO) Solar Cells for All-Transparent Module Integration. *Sol. Energy Mater. Sol. Cells* **2017**, *170*, 246–253.

[7] Arafat, M. M.; Dinan, B.; Akbar, S. A.; Haseeb, A. S. M. A. Gas Sensors Based on One Dimensional Nanostructured Metal-Oxides: A Review. *Sensors* **2012**, *12 (6)*, 7207–7258.

[8] Comini, E.; Baratto, C.; Faglia, G.; Ferroni, M.; Ponzoni, A.; Zappa, D.; Sberveglieri, G. Metal Oxide Nanowire Chemical and Biochemical Sensors. *J. Mater. Res.* **2013**,

28 (21), 2911–2931.

[9] Comini, E.; Sberveglieri, G. Metal Oxide Nanowires as Chemical Sensors. *Mater. Today* **2010**, *13 (7–8)*, 36–44.

[10] M.F.M.; Md Arshad, M. K.; Ruslinda, A. R.; Gopinath, S. C. B.; Nuzaihan M.N., M.; Adzhri, R.; Hashim, U.; Lam, H. Y. Substrate-Gate Coupling in ZnO-FET Biosensor for Cardiac Troponin I Detection. *Sens. Actuators B Chem.* **2017**, *242*, 1142–1154.

[11] Ahmad, R.; Mahmoudi, T.; Ahn, M.-S.; Hahn, Y.-B. Recent Advances in Nanowires-Based Field-Effect Transistors for Biological Sensor Applications. *Biosens. Bioelectron.* **2018**, *100*, 312–325.

[12] Ahn, J.-H.; Choi, S.-J.; Han, J.-W.; Park, T. J.; Lee, S. Y.; Choi, Y.-K. Double-Gate Nanowire Field Effect Transistor for a Biosensor. *Nano Lett.* **2010**, *10 (8)*, 2934–2938.

[13] Aroonyadet, N.; Wang, X.; Song, Y.; Chen, H.; Cote, R. J.; Thompson, M. E.; Datar, R. H.; Zhou, C. Highly Scalable, Uniform, and Sensitive Biosensors Based on Top-Down Indium Oxide Nanoribbons and Electronic Enzyme-Linked Immunosorbent Assay. *Nano Lett.* **2015**, *15 (3)*, 1943–1951.

[14] Drobek, M.; Kim, J.-H.; Bechelany, M.; Vallicari, C.; Julbe, A.; Kim, S. S. MOF-Based Membrane Encapsulated ZnO Nanowires for Enhanced Gas Sensor Selectivity. *ACS Appl. Mater. Interfaces* **2016**, *8 (13)*, 8323–8328.

[15] Zeng, H.; Takahashi, T.; Kanai, M.; Zhang, G.; He, Y.; Nagashima, K.; Yanagida, T. Long-Term Stability of Oxide Nanowire Sensors via Heavily Doped Oxide Contact. *ACS Sens.* **2017**, *2 (12)*, 1854–1859.

[16] Zhou, J.; Xu, N. S.; Wang, Z. L. Dissolving Behavior and Stability of ZnO Wires in Biofluids: A Study on Biodegradability and Biocompatibility of ZnO Nanostructures.

Adv. Mater. **2006**, *18 (18)*, 2432–2435.

[17] Patolsky, F.; Zheng, G.; Lieber, C. M. Nanowire-Based Biosensors. *Anal. Chem.* **2006**, *78 (13)*, 4260–4269.

[18] Duan, X.; Li, Y.; Rajan, N. K.; Routenberg, D. A.; Modis, Y.; Reed, M. A. Quantification of the Affinities and Kinetics of Protein Interactions Using Silicon Nanowire Biosensors. *Nat. Nanotechnol.* **2012**, *7 (6)*, 401–407.

[19] Miller, D. R.; Akbar, S. A.; Morris, P. A. Nanoscale Metal Oxide-Based Heterojunctions for Gas Sensing: A Review. *Sens. Actuators B Chem.* **2014**, *204*, 250–272.

[20] Walker, J. M.; Akbar, S. A.; Morris, P. A. Synergistic Effects in Gas Sensing Semiconducting Oxide Nano-Heterostructures: A Review. Sens. *Actuators B Chem.* **2019**, *286*, 624–640.

[21] Hwang, I.-S.; Kim, S.-J.; Choi, J.-K.; Choi, J.; Ji, H.; Kim, G.-T.; Cao, G.; Lee, J.-H. Synthesis and Gas Sensing Characteristics of Highly Crystalline ZnO–SnO2 Core–Shell Nanowires. *Sens. Actuators B Chem.* **2010**, *148 (2)*, 595–600.

[22] Yang; Kim, D. S.; Knez, M.; Scholz, R.; Berger, A.; Pippel, E.; Hesse, D.; Gösele, U.; Zacharias, M. Influence of Temperature on Evolution of Coaxial ZnO/Al 2 O 3 One-Dimensional Heterostructures: From Core−Shell Nanowires to Spinel Nanotubes and Porous Nanowires. *J. Phys. Chem. C* **2008**, *112 (11)*, 4068–4074.

[23] Rackauskas, S.; Barbero, N.; Barolo, C.; Viscardi, G. ZnO Nanowire Application in Chemoresistive Sensing: A Review. *Nanomaterials* **2017**, *7 (11)*, 381.

[24] Tian, B.; Lieber, C. M. Nanowired Bioelectric Interfaces: Focus Review. *Chem. Rev.* **2019**, *119 (15)*, 9136–9152.

[25] Liu, B.; Liu, J. Sensors and Biosensors Based on Metal Oxide Nanomaterials. *TrAC Trends Anal. Chem.* **2019**, *121*, 115690.

[26] Chen, X.; Wong, C. K. Y.; Yuan, C. A.; Zhang, G. Nanowire-Based Gas Sensors. *Sens. Actuators B Chem.* **2013**, *177*, 178–195.

[27] Blesa, M. A.; Weisz, A. D.; Morando, P. J.; Salfity, J. A.; Magaz, G. E.; Regazzoni, A. E. The Interaction of Metal Oxide Surfaces with Complexing Agents Dissolved in Water. Coord. *Chem. Rev.* **2000**, *196 (1)*, 31–63.

[28] Limo, M. J.; Sola-Rabada, A.; Boix, E.; Thota, V.; Westcott, Z. C.; Puddu, V.; Perry, C. C. Interactions between Metal Oxides and Biomolecules: From Fundamental Understanding to Applications. *Chem. Rev.* **2018**, *118 (22)*, 11118–11193.

[29] Xu, L.; Zhao, Y.; Owusu, K. A.; Zhuang, Z.; Liu, Q.; Wang, Z.; Li, Z.; Mai, L. Recent Advances in Nanowire-Biosystem Interfaces: From Chemical Conversion, Energy Production to Electrophysiology. *Chem* **2018**, *4 (7)*, 1538–1559.

[30] Ahmad, R.; Ahn, M.-S.; Hahn, Y.-B. ZnO Nanorods Array Based Field-Effect Transistor Biosensor for Phosphate Detection. *J. Colloid Interface Sci.* **2017**, *498*, 292–297.

[31] Bhaumik, A.; Shearin, A. M.; Delong, R.; Wanekaya, A.; Ghosh, K. Probing the Interaction at the Nano–Bio Interface Using Raman Spectroscopy: ZnO Nanoparticles and Adenosine Triphosphate Biomolecules. *J. Phys. Chem. C* **2014**, *118 (32)*, 18631–18639.

[32] Bica-Pop, C.; Cojocneanu-Petric, R.; Magdo, L.; Raduly, L.; Gulei, D.; Berindan-Neagoe, I. Overview upon MiR-21 in Lung Cancer: Focus on NSCLC. *Cell. Mol. Life Sci.* **2018**, *75 (19)*, 3539–3551.

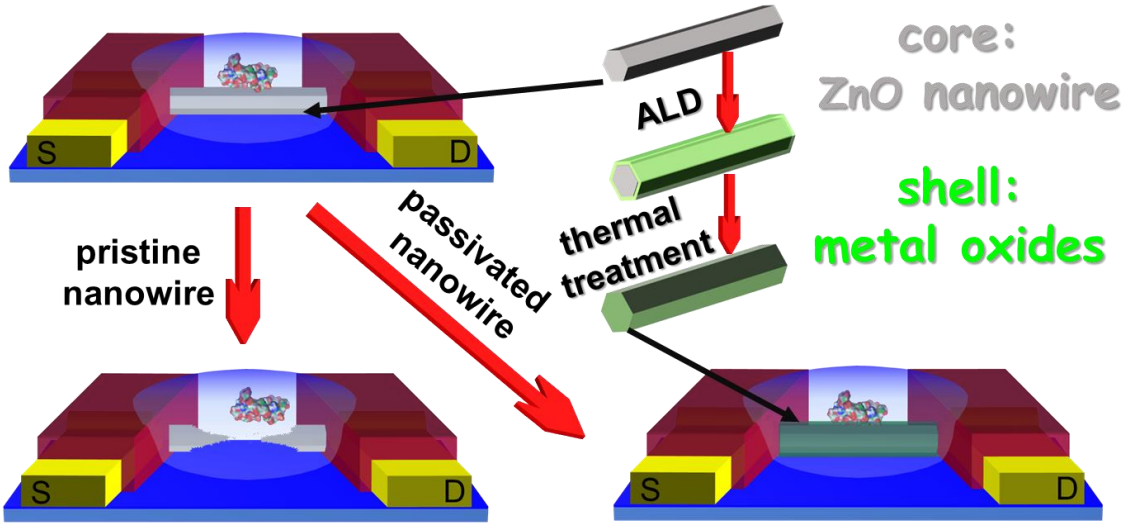

Figure 4-1 Schematic diagram of stabilized metal oxide core-shell nanowire towards biosensing.

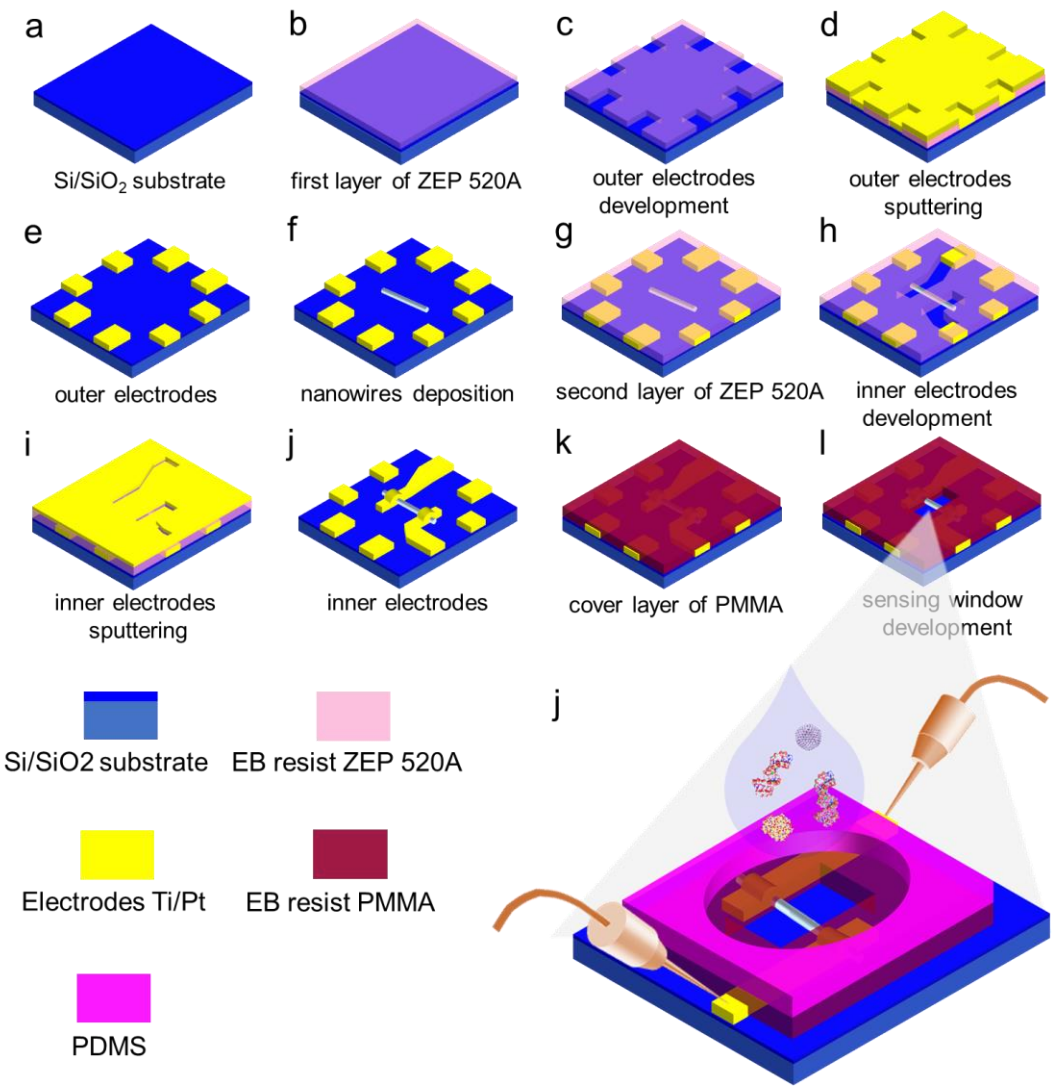

Figure 4-2 Flowchart of individual nanowire device fabrication by EB.

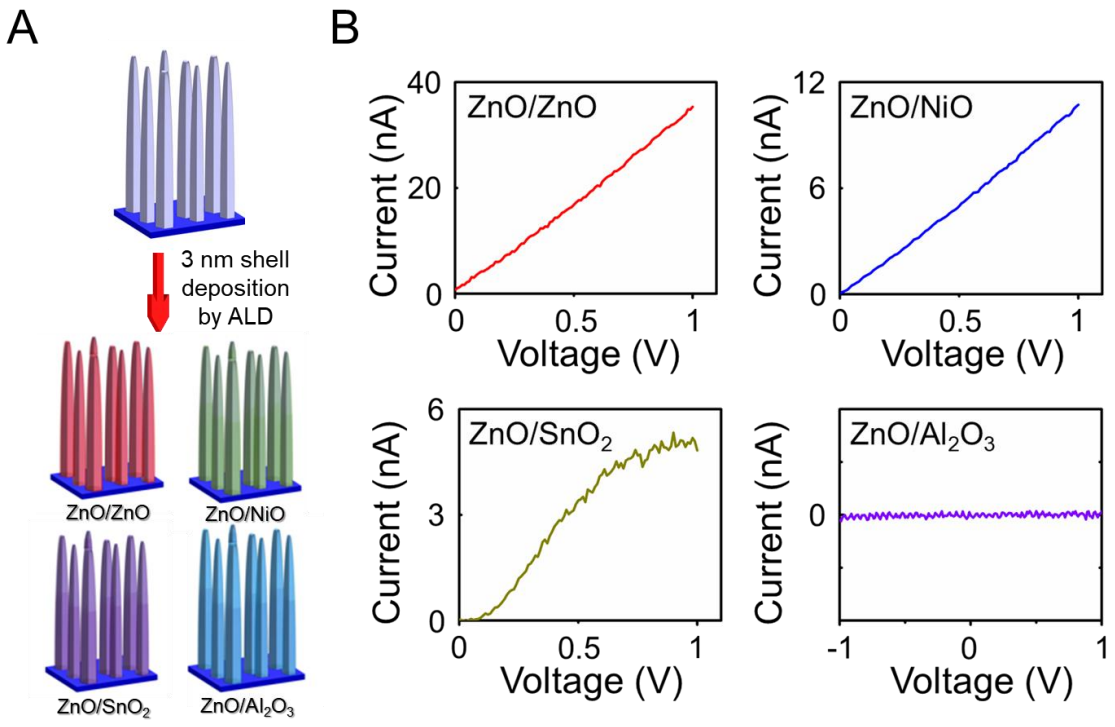

Figure 4-3 ZnO/metal oxides core-shell fabricated using ALD and their nanostructures I-V curves. **A.** Schematic diagram of ZnO nanowires cover by metal oxides deposition layer. **B.** ZnO/metal oxides core-shell nanostructures I-V curves.

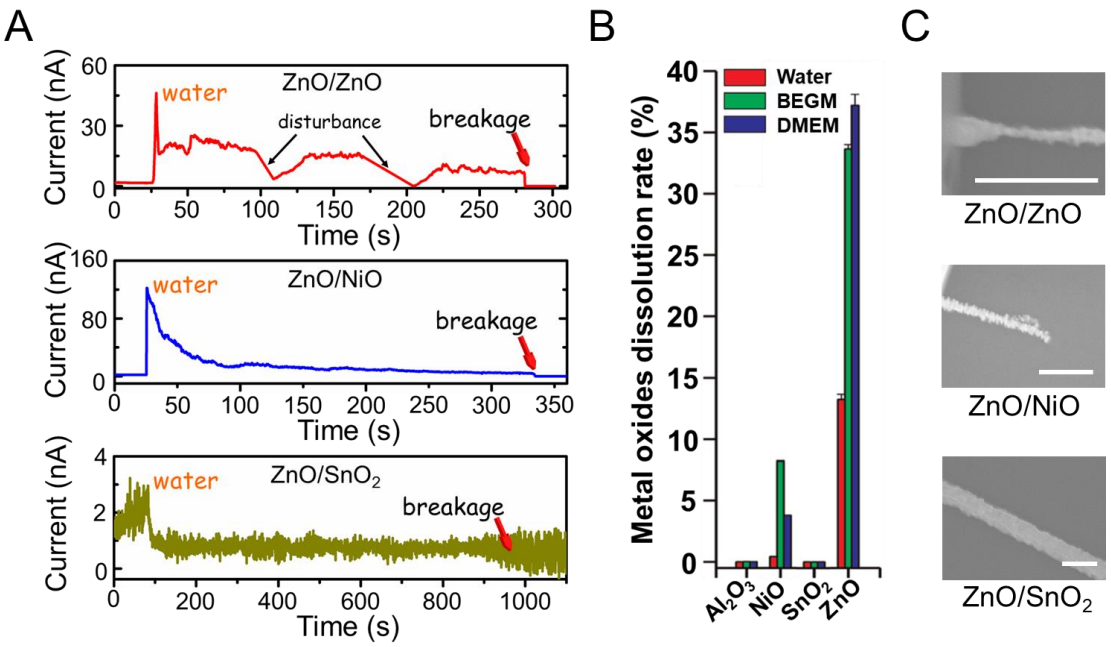

Figure 4-4 ZnO nanowire passivation by deposition of stable metal oxides shell. **A.** Current measurement of ZnO/metal oxides core-shell nanodevices in water condition. **B.** Metal oxide nanoparticles dissolution rate, refer to [25]. **C.** SEM images of ZnO/metal oxides core-shell nanodevices after measurement in water, scale bar: 500 nm.

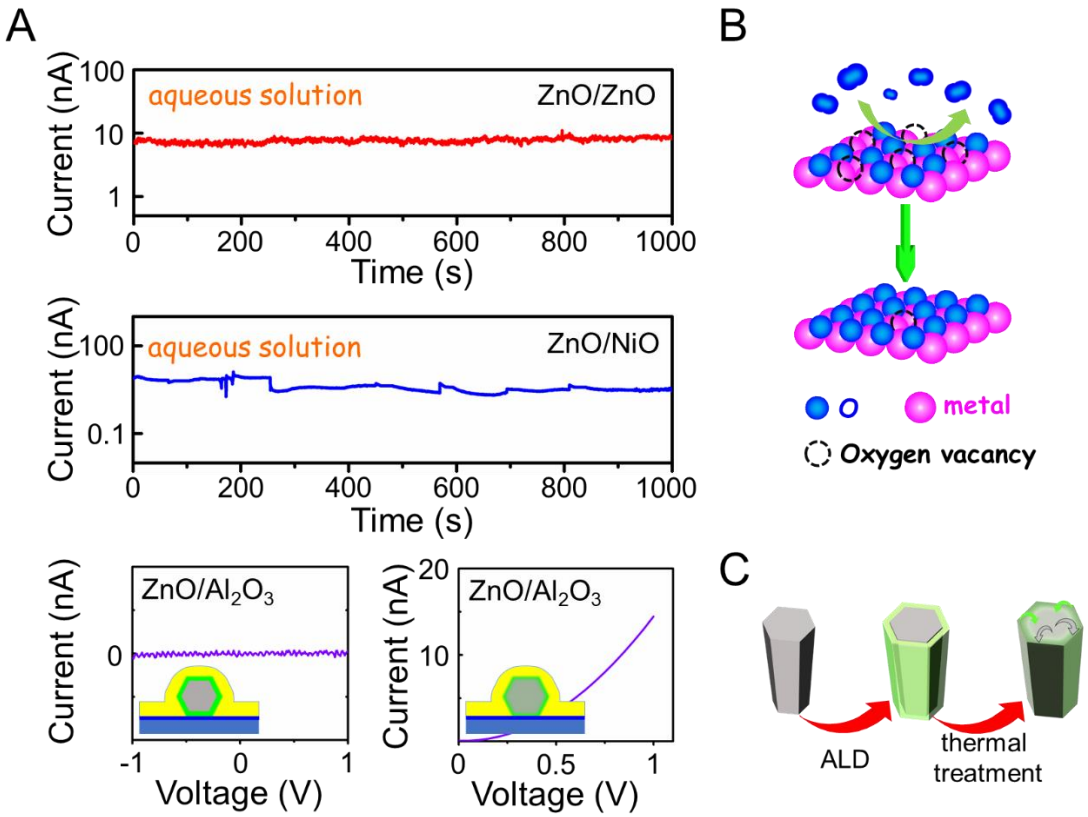

Figure 4-5 ZnO nanowire passivation by deposition of stable metal oxides shell and thermal treatment. **A.** Current measurement of ZnO/metal oxides core-shell nanodevices. **B.** Schematic diagram of metal oxide thermal treatment in atmosphere. **C.** Schematic diagram of metal atoms diffusion in ZnO/metal oxides core-shell nanowire during thermal treatment.

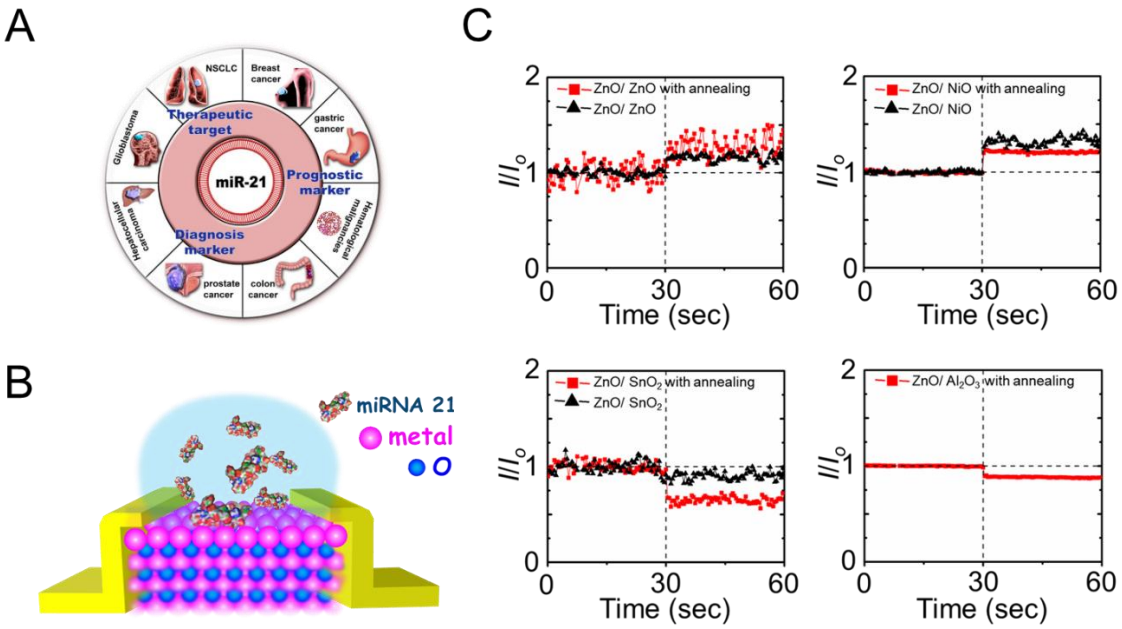

Figure 4-6 Thermal annealing derived stabilization of metal oxide core-shell nanowire towards sensing response to miRNA 21. **A.** miRNA 21 is an important diagnosis/prognostic marker and therapeutic target for precision medicine. **B.** Schematic diagram of mi RNA 21 sensing. **C.** Metal oxide core-shell nanowire sensing response to miRNA 21, miRNA 21 is injected at the 30 s.

CHAPTER V

Concluding Remarks and Future Perspective

Concluding Remarks and Future Perspectives

5.1 Concluding Remarks

In this thesis, we overcome several constrains in zinc oxide nanowires growth and biosensing application. In chapter II, we first present a seed layer engineering strategy to control the morphology and intrinsic crystallinity of ZnO nanowires via a hydrothermal method. The process in which nanowires grow from prepared seed template layer, ammonia is added in growth system to promotes growth of nanowires. Although the effect of ammonia on the nanowire growth has been intensively investigated, an influence for the seed layer, which governs the initial nanowire growth, is rarely discussed. Here current part of this thesis demonstrates that ammonia strongly affects the seed layer as well as the following nanowire growth. When increasing the ammonia concentration, the nanowire density first increases and then decreases while the nanowire growth rate keeps increasing. Experimental results and thermodynamic calculations as to the initial growth process reveal that the transformation of seed layer induced by ammonia prior to the nucleation critically determines the nanowire density and thus also influences the following nanowire growth. Present results highlight the critical importance to discuss the variation of seed layer in ammonia-contained hydrothermal synthesis and suggest a novel seed engineering approach for tailoring the ZnO nanowire growth, and even physical property. In chapter III, we describe a manageable procedure to embed individual ZnO nanowire in device, and explore the electron transport property of it. Based on the results in Chapter II, sparse ZnO nanowire array with aspect ratio of ca. 120 and growth rate of 1 μm/h is synthesized by controlling density of seeds by ammonia and polyethyleneimine at initial stage of nanowire growth,

and prolong the growth period by refreshing nutrient solution. The spatially-separated nanowires were cut off from growth substrate unbrokenly, and thus facilitate to construct a single-nanowire device by photolithography. The device exhibited a linear current-voltage characteristic associated with ohmic contact between ZnO nanowire and electrodes. The device further demonstrated reliable photoresponse with an I_{UV}/I_{dark} of ~100 to ultraviolet light irradiation. In chapter IV, we propose the establishment of ZnO-based individual nanodevices with high stability and enhanced response towards biomolecules miRNA 21. The implementation approach is that, atomic layer deposition (ALD) technology boosted constructure of ZnO/ Al_2O_3, ZnO/ SnO_2, and ZnO/ NiO core-shell nanowires. Nanodevices embedding the core-shell nanowires were responded to miRNA 21 in aqueous environment. Formation and thermal treatment of core-shell nanostructures not only enhanced the electrical response of ZnO nanowire to biomolecular potentially, thermal annealing but also caused diffusion of deposited metal oxide layer on ZnO nanowire surface increased stability of nanowire. Comparison of different response signal, a hypothesis was presented to further understand the sensing mechanism between metal oxide surface and miRNA. Based on a mature research of core-shell nanodevices, the selective fingerprinting of miRNAs by material-dependent nanosensors arrays is expected to realize.

5.2 Future Perspective

As mentioned above, we want to establish a mature platform base on core-shell nanodevices, to realize selective fingerprinting of miRNAs. Although our previous results show that the deposition of stable metal oxides and thermal treatment are able to increase the stability of nanowire and enhance response to biomolecule, there is no specificity or selectivity. One more thing should be noted that the biomarkers of cancer or inflammation are various. That

means, for one individual nanowire device cannot make a diagnosis. It is necessary to get a “3D” profile of the cancer or inflammation, then give the diagnosis. Therefore, there is an eager demand to multiple data acquisition. Nanowires possess the advantage of miniaturization, with specifical modification, could be integrated in an array. The integration would sense to several biomarkers at once, and draw a “3D” profile of the biomarker level variations. Finally, after integrating the data, and make a more accurate diagnosis. Our priority is to resolve the problem of selectivity, which is basic of big data acquisition.

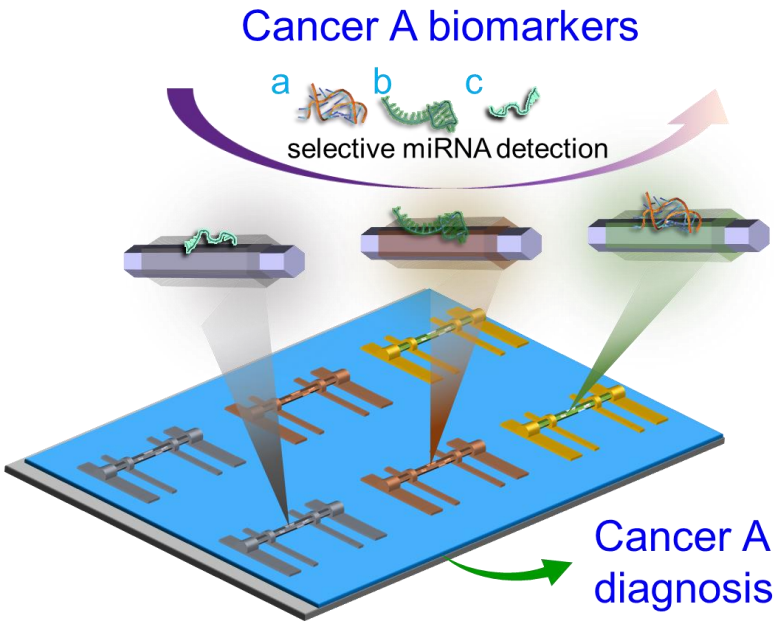

Figure 5 Integration of selective individual nanowire sensor towards cancer diagnosis.

ACKNOWLEDGEMENT

First and foremost, I sincerely express my gratitude to Prof. Yoshinobu Baba of Department of Biomolecular Engineering, Graduate School of Engineering, Nagoya University for his careful guidance, selfless supports, constructive discussion, and affable encouragement. His profound learning, life experience, and great perception direct my advance and show me the way forward.

Then, I want to express my gratitude to Prof. Takao Yasui for his continuous encouragements, adequate supports, multi-dimensional discussion and suggestions. His flexible thinking and innovative ideas deeply affect and promote my research.

I wish to thank Prof. Takeshi Yanagida (Department of Applied Chemistry, School of Engineering, The University of Tokyo) and Prof. Kazuki Nagashima (Department of Applied Chemistry, School of Engineering, The University of Tokyo) for their constructive suggestions and experimental assistance. I wish to express my thanks to Prof. Noritada Kaji of Department of Applied Chemistry, Faculty of Engineering, Kyushu University for his e kind supports. I wish to thank Dr. Taisuke Shimada (Assistant Professor now in Graduate School of Engineering, Nagoya University), Dr. Akihide Arima, Dr. Hiroshi Yukawa, and Dr. Daisuke Onoshima for their scientific discussions and suggestions. I also wish to thank Prof. Mitsuo Hara (Department of Molecular and Macromolecular Chemistry, Graduate School of Engineering, Nagoya University) for his benevolent effort in X-ray diffraction and Atomic Force Microscope test. I would like to thank Dr. Zetao Zhu, Dr. Hiromi Takahashi, and Dr. Musa, Marina Binti for their kind suggestions and encouragement. I also would like to thank Mr. Masafumi Horiuchi for his kind share of experiences in

nanowires synthesis. I want to give my thanks to Mr. Hiroki Naito and Mr. Tsuyoshi Naganawa for their helps in apparatuses operation. Furthermore, I would like to thank all current and previous members in Baba Lab for their kind assistances not only in study bust also in everyday life. I want to express my thanks to the support from Japan Science and Technology Agency (JST), Japan Society for the Promotion of Science (JSPS), and the Ministry of Education, Culture, Sports, Science and Technology (MEXT). In addition, I would like to express my gratitude to my family, for their understanding and moral supports during my Ph. D course. At last, I want to express my thanks sincerely again to kind people mention above, and to all people who give me their selfless supports during my Ph. D course.

List of publications

Journal paper

1. "Ammonia-Induced Seed Layer Transformations in a Hydrothermal Growth Process of Zinc Oxide Nanowires"

   Quanli Liu, Takao Yasui, Kazuki Nagashima, Takeshi Yanagida, Mitsuo Hara, Masafumi Horiuchi, Zetao Zhu, Hiromi Takahashi, Taisuke Shimada, Akihide Arima, and Yoshinobu Baba

   The Journal of Physical Chemistry C, https://dx.doi.org/10.1021/acs.jpcc.0c05490

2. "Photolithographically Constructed Single ZnO Nanowire Device and Its Ultraviolet Photoresponse"

   Quanli Liu, Takao Yasui, Kazuki Nagashima, Takeshi Yanagida, Masafumi Horiuchi, Zetao Zhu, Hiromi Takahashi, Taisuke Shimada, Akihide Arima, and Yoshinobu Baba

   Analytical Sciences **36(9)**, 1125-1129 (2020)

Conference paper

1. "Hybridization-Based DNA Analysis by Self-Heating Nanowire Microfluidic Devices"

   H. Takahashi, T. Yasui, K. Shinjo, **Q. Liu,** T. Shimada, N. Kaji, H. Kashida, and Y. Baba

   The 23rd International Conference on Miniaturized Systems for Chemistry and Life Sciences,

   Basel, Switzerland, 2019, 720-721 (Conference paper)

Conferences

1“Hydrothermal synthesis of low dense array of long ZnO nanowires”

Quanli Liu, Takao Yasui, Noritada Kaji, and Yoshinobu Baba

The 99th CSJ Annual Meeting, Chiba, Japan, 2019, 3, 16-19 (Oral presentation)

2. “Hydrothermal Synthesis of Single Long ZnO Nanowire”

Quanli Liu, Takao Yasui, Noritada Kaji, and Yoshinobu Baba

The 11th International Symposium on Microchemistry and Microsystems, Shaanxi, China, 2019, 5,17-20 (Oral presentation)

Scientific Awards

CSJ Student Presentation Award

Quanli Liu

“Hydrothermal synthesis of low dense array of long ZnO nanowires”

The 99th CSJ Annual Meeting, Chiba, Japan, 2019, 3, 16-19 (Oral presentation)